ICEBERG CALVING DYNAMICS OF JAKOBSHAVN ISBRÆ, GREENLAND

By

Jason Michael Amundson

RECOMMENDED:

_____

_____

_____

_____

_____

Advisory Committee Chair

_____

Chair, Department of Geology and Geophysics

APPROVED:

_____

Dean, College of Natural Science and Mathematics

_____

Dean of the Graduate School

_____

Date

ICEBERG CALVING DYNAMICS OF JAKOBSHAVN ISBRÆ, GREENLAND

A

THESIS

Presented to the Faculty

of the University of Alaska Fairbanks

in Partial Fulfillment of the Requirements

for the Degree of

DOCTOR OF PHILOSOPHY

By

Jason Michael Amundson, B.S., M.S.

Fairbanks, Alaska

May 2010

Abstract

Jakobshavn Isbræ, a fast-flowing outlet glacier in West Greenland, began a rapid retreat in the late 1990's. The glacier has since retreated over 15 km, thinned by tens of meters, and doubled its discharge into the ocean. The glacier's retreat and associated dynamic adjustment are driven by poorly-understood processes occurring at the glacier-ocean interface. These processes were investigated by synthesizing a suite of field data collected in 2007–2008, including timelapse imagery, seismic and audio recordings, iceberg and glacier motion surveys, and ocean wave measurements, with simple theoretical considerations. Observations indicate that the glacier's mass loss from calving occurs primarily in summer and is dominated by the semi-weekly calving of full-glacier-thickness icebergs, which can only occur when the terminus is at or near flotation. The calving icebergs produce long-lasting and far-reaching ocean waves and seismic signals, including "glacial earthquakes". Due to changes in the glacier stress field associated with calving, the lower glacier instantaneously accelerates by $\sim$3% but does not episodically slip, thus contradicting the originally proposed glacial earthquake mechanism. We furthermore showed that the predominance of calving during summer can be attributed to variations in the strength of the proglacial ice mélange (dense pack of sea ice and icebergs). Sea ice growth in winter stiffens the mélange and prevents calving; each summer the mélange weakens and calving resumes. Previously proposed calving models are unable to explain the terminus dynamics of Jakobshavn Isbræ (and many other calving glaciers). Using our field observations as a basis, we developed a general framework for iceberg calving models that can be applied to any calving margin. The framework is based on mass continuity, the assumption that calving rate and terminus velocity are not independent, and the simple idea that terminus thickness following a calving event is larger than terminus thickness at the event onset. Although the calving framework does not constitute a complete calving model, it provides a guide for future attempts to define a universal calving law.

Table of Contents

Page

List of Figures

Page

List of Tables

List of Other Materials

List of Appendices

Acknowledgements

I write this as I am halfway through my eighth year in Fairbanks. Even though I've lived most of this time in what some people might say are dry, poorly-insulated, and poorly-heated cabins, I really "can't complain" about the time that I've spent here (pardon my Minnesotan). In fact, I know that I'm going to miss this place and its people a whole heck of a lot once I leave.

I've been fortunate to have many colleagues that I also consider friends, including my advisor Martin Truffer. Martin encouraged me to develop my own ideas and challenged me to finish them; I find it difficult to imagine an advisor that could have better prepared me for the future. (Thanks also Dana for letting us have so much fun in Greenland!) The rest of my committee was equally supportive. Roman Motyka taught me to remember the data, Ed Bueler (excitedly) answered my trivial math questions and advised me on framing my work in the context of ice sheet models, Regine Hock offered her brutally honest opinions of my manuscript drafts ("This is boring!"), and Erin Pettit rightfully questioned some of my ideas. My thesis also strongly benefited from discussions with Mark Fahnestock, who at times was essentially a co-advisor. He taught me something about networking and creativity, and never rejected any of my ideas outright, even when he maybe should have.

Field work and data analysis would not have been as successful or enjoyable without Martin "Tinu" Lüthi, Jed Brown, and Dave Podrasky. Tinu taught me some great Swiss expressions, im prinzip, and amazed me with his cheese consumption. David Maxwell and Guðfinna "Tolly" Aðalgeirsdóttir also assisted with field work, and Dale Pomraning helped prepare equipment.

Throughout my thesis I explored topics that were outside the realm of traditional glaciology. Mike West, Celso Reyes, and Helena Buurman held my hand as I navigated the dark world of seismology and somehow survived, while Shad O'Neel, Fabian Walter, and Victor Tsai enthusiastically discussed the finer points of glacier seismology. David Holland and Doug MacAyeal exposed me to the exciting field of polar oceanography. Chris Larsen shared an interest in glacier-ocean-solid earth interactions, and also had many useful tips

for processing GPS data and other large data sets. The willingness of these people to share their time and ideas with me has certainly enriched my education. I am happy for the opportunity to work in such an open and fun enviroment.

This project gave me the chance to visit and work on a highly dynamic, unique, and relatively well-studied glacier. The pioneering work of Keith Echelmeyer and Will Harrison, among others, elucidated many of the glacier's unique features. They studied nearly every facet of the glacier, but luckily for me did not write any manuscripts on iceberg calving events and their impact on the fjord and solid earth (thanks Keith!).

While in Greenland I participated in outreach activities in the town of Ilulissat, where I worked closely with Naja Habermann and Kirsten Strandgaard. It was a very enjoyable collaboration (thanks for the dog sled trips!), and one that I hope we can continue well into the future.

Early in my Ph.D. I received a travel grant to work on Tasman Glacier, New Zealand, on a project unrelated to my thesis. Andrew Mackintosh, Brian Anderson, and Tom Paulin were very accomodating hosts. Maybe this year I'll have time to write up that data...

I have shared lab space, coffee-stimulated discussions, and ski trips with many other glaciers folks over the years, including Anthony Arendt, Andy Aschwanden (thanks for the LaTeX help), Tim Bartholomaus, Indrani Das, Jason Geck, Marijke Habermann, Sam Herreid, John Hulth, Syosaku Kanamori, Joe Kennedy, Constantine Khroulev (thanks for the math help), Laura LeBlanc, Bob McNabb, Valentina Radić (Heck!), Brent Ritchie, Barbara Trüssel, By Valentine, and Sandy "Lee" Zirnheld.

I'd like to thank my family for putting up with me living so far away and my friends (in addition to those listed above) for providing me with distractions from science. I am especially grateful to Inari for following me to Alaska and constantly amusing me with her creativity. Even though I didn't always want to hear her graphic design advice, she was always right.

Finally, "qujanaq" to Greenland and its people for transforming my Ph.D. into a wonderful life experience. I hope to see you again!

Chapter 1
Introduction

1.1 Background

The recent calving retreat and coincident flow acceleration of outlet glaciers in Greenland and Antarctica [*De Angelis and Skvarca*, 2003; *Joughin et al.*, 2004; *Rignot et al.*, 2004; *Howat et al.*, 2008] has demonstrated that ice sheets can evolve rapidly in response to oceanic and atmospheric forcings [*Truffer and Fahnestock*, 2007]. Models have traditionally assumed, however, that ice sheets evolve slowly over millenia. The ability of current ice sheet models to predict future sea level variations is therefore suspect, due in large part to a poor understanding and parameterization of iceberg calving processes. Attempts to define a universal calving law are hindered by difficulties in making direct measurements of calving due to safety concerns, the episodic nature of calving, and the vast size and remote location of many calving margins. Investigations are further confounded by the wide variety of calving phenomena, including the sub-hourly detachment of small ice blocks from grounded, temperate glaciers [*O'Neel et al.*, 2003, 2007], the roughly decadal calving of giant tabular icebergs (with horizontal dimensions of 10–100 km) from floating ice shelves [*Lazzara et al.*, 1999], and the catastrophic collapse of thin ice shelves within a matter of days to weeks [*Rott et al.*, 1996; *Scambos et al.*, 2000; *Braun et al.*, 2009; *Braun and Humbert*, 2009].

Central to the calving "problem" is the realization that calving, glacier flow, and glacier geometry are related through highly nonlinear and nontrivial relationships. Over annual time scales, calving rate and terminus velocity tend to scale with each other, such that the rate of glacier length change is one to two orders of magnitude smaller than calving rate or terminus velocity [*Van der Veen*, 1996]; the observation that calving rate and terminus velocity are two numbers of similar magnitude that almost exactly cancel indicates that they are not independent. This is not entirely surprising because calving is inherently controlled by ice fracture and subsequent propagation of crevasses and/or rifts through extensional processes, and calving events change the geometry, and therefore stress distribution, of

the lower glacier. Although these processes are poorly understood, it is at least clear that calving processes should not be investigated independently of glacier flow dynamics [see also *Benn et al.*, 2007a].

Terminus dynamics are additionally affected by numerous secondary processes. For example fjord convection, which is driven by subglacial discharge, draws warm saline water toward the glacier terminus where it mixes with freshwater, rises to the fjord surface, and flows down fjord as a relatively thin surface plume. The upwelling plume of mixed fresh and saline water melts the glacier terminus, and can therefore enable calving by changing the buoyant torques on the vertical face of the terminus [*Motyka et al.*, 2003] and/or reducing the terminus thickness, and therefore strength, if the terminus is floating [e.g., *Holland et al.*, 2008]. Fjord convection similarly impacts the thickness and strength of sea ice cover or ice mélanges (dense packs of brash ice and icebergs), which have been postulated to inhibit calving [e.g., *Birnie and Williams*, 1985; *Higgins*, 1991; *Reeh et al.*, 2001]. Thus changes in ocean temperature or processes controlling subglacial discharge, such as surface melting, can strongly impact terminus dynamics. Other processes that may influence calving include melt-driven propagation of surface crevasses [*Scambos et al.*, 2000] and flexure and associated fatigue, fracture, and break-up of ice shelves by various types of ocean waves [e.g., *Cathles et al.*, 2009, and references therein].

Untangling the numerous glacier-ocean feedbacks is clearly a major endeavour. Even if all of the processes controlling calving were fully understood, though, there would still remain the daunting task of reconciling the high temporal and spatial resolution necessary to model these processes with the computational constraints of ice sheet models. An alternative is to seek a parameterization of calving that is sufficiently general to be applicable to any calving margin, yet sufficiently simple to be implementable in ice sheet models. Previous efforts to parameterize calving include (1) relating calving rate of grounded glaciers to water depth at the terminus [*Brown et al.*, 1982], (2) continuously adjusting the terminus position so that terminus thickness always equals some value given by a calving criterion [*Van der Veen*, 1996; *Vieli et al.*, 2000; Vieli and others, 2001; *Benn et al.*, 2007a,b], and (3)

relating calving rate of ice shelves to their thickness, width, and longitudinal strain rate [*Alley et al.*, 2008]. Although progress has been made in recent years, none of the previous efforts can fully address the wide range in size and occurrence frequency of calving events.

1.2 Project and objectives

To investigate processes influencing calving and associated changes in glacier flow, we began a comprehensive field campaign in 2006 at Jakobshavn Isbræ, an outlet glacier that drains roughly 6% of the Greenland Ice Sheet [*Bindschadler*, 1984]. Over the last fifteen years the glacier has thinned by tens of meters [*Abdalati et al.*, 2001; *Thomas et al.*, 2003], doubled its ice discharge into the ocean [*Joughin et al.*, 2004], and retreated over 10 km, losing an extensive floating tongue in the process [*Podlech and Weidick*, 2004; *Csatho et al.*, 2008]. Both the present flow speed and retreated terminus position are maximums in the observational record. Due to the glacier's large ice flux, there is concern that the observed acceleration of the glacier may compromise the stability of the Greenland Ice Sheet. In addition to being an important outlet glacier in Greenland, Jakobshavn Isbræ makes a good site for studying calving processes because it is easily accessible from the nearby town of Ilulissat, prior knowledge of the glacier's dynamics and geometry has been provided from several previous studies, the glacier is well-known for regularly calving large icebergs (large calving icebergs are easier to observe than small icebergs), and very few detailed studies of calving have been conducted on any of Greenland's fast-flowing outlet glaciers. The project aimed to (1) characterize calving events and their impacts, (2) investigate any unique processes that could give insight into calving dynamics, and (3) use our observations from (1) and (2) to improve upon previous attempts to parameterize calving.

Our field campaign consisted of timelapse photography of the glacier and fjord, iceberg and glacier motion surveys with optical surveying methods and GPS receivers, acoustic and seismic recordings of calving events, and ocean wave measurements. Our observations suggest that Jakobshavn Isbræ (and presumably similar outlet glaciers in Greenland) represents a distinct and previously undefined class of calving glaciers. Calving events

and their impact on the glacier, fjord, and solid earth are described in detail in Chapter 2, which was published in Geophysical Research Letters.

An interesting feature of Jakobshavn Isbræ is the presence of a dense mélange of icebergs and brash ice in the proglacial fjord that persists year round. Visual observations suggest that the mélange is essentially a weak, poorly-sorted, granular ice shelf, and is therefore capable of influencing glacier dynamics by exerting back pressure on the glacier terminus [see also *Thomas*, 1979; *Geirsdóttir et al.*, 2008]. Seasonal variations in mélange strength can occur as sea ice grows and decays. In Chapter 3, which was published in the Journal of Geophysical Research, we use field measurements and theoretical considerations to investigate the dynamics of the mélange and interactions between the mélange, glacier, and fjord.

Chapters 2 and 3 raise the following broad questions (among others):

1. Why does the terminus of Jakobshavn Isbræ behave differently from other documented calving margins (such as temperate tidewater glaciers in Alaska or expansive ice shelves in Antarctica)?
2. What general form should a calving model assume in order to adequately describe the terminus behavior of Jakobshavn Isbræ?

With these questions in mind, we developed a broad framework for iceberg calving models that can be applied to any calving margin. The framework is based on mass continuity, the observation that terminus velocity and calving rate tend to scale with each other [*Van der Veen*, 1996], and the simple idea that terminus thickness increases during a calving event. Although the framework does not constitute a complete calving model, it is highly versatile, can be applied to any calving margin, and provides a guide for future attempts to parameterize calving. The framework is presented in Chapter 4, which has been submitted for publication in the Journal of Glaciology.

Finally, Chapter 5 summarizes the key findings of this thesis and provides an outlook for future studies of calving in Greenland and elsewhere.

Chapter 2
Glacier, fjord, and seismic response to recent large calving events, Jakobshavn Isbræ, Greenland [1]

Abstract

The recent loss of Jakobshavn Isbrae's extensive floating ice tongue was accompanied by a change in near terminus behavior. Calving currently occurs primarily in summer from a grounded terminus, involves the detachment and overturning of several icebergs within 30-60 min, and produces long-lasting and far-reaching ocean waves and seismic signals, including "glacial earthquakes". Calving also increases near-terminus glacier velocities by $\sim$3% but does not cause episodic rapid glacier slip, thereby contradicting the originally proposed glacial earthquake mechanism. We propose that the earthquakes are instead caused by icebergs scraping the fjord bottom during calving.

2.1 Introduction

During the past decade Jakobshavn Isbræ (Greenlandic name: Sermeq Kujalleq) and numerous other outlet glaciers draining from the Greenland Ice Sheet have dramatically thinned, accelerated, and retreated, in some cases doubling their iceberg calving rates [*Abdalati et al.*, 2001; *Rignot and Kanagaratnam*, 2006]. Although ice discharge accounts for roughly two-thirds of the mass loss from the Greenland Ice Sheet [*Rignot and Kanagaratnam*, 2006], calving processes, terminus stability, and related changes in glacier motion remain poorly understood. Consequently, controls on terminus dynamics have not been fully incorporated into predictions of Greenland's future mass balance and therefore current models may considerably underestimate future sea level rise [*IPCC*, 2007; *Rahmstorf*, 2007].

[1] Published as Amundson, J.M, M. Truffer, M.P. Lüthi, M. Fahnestock, M. West, and R.J. Motyka, 2008. Glacier, fjord, and seismic response to recent large calving events, Jakobshavn Isbræ, Greenland. *Geophys. Res. Lett.*, *35*(L22501), doi:10.1029/2008GL035281.

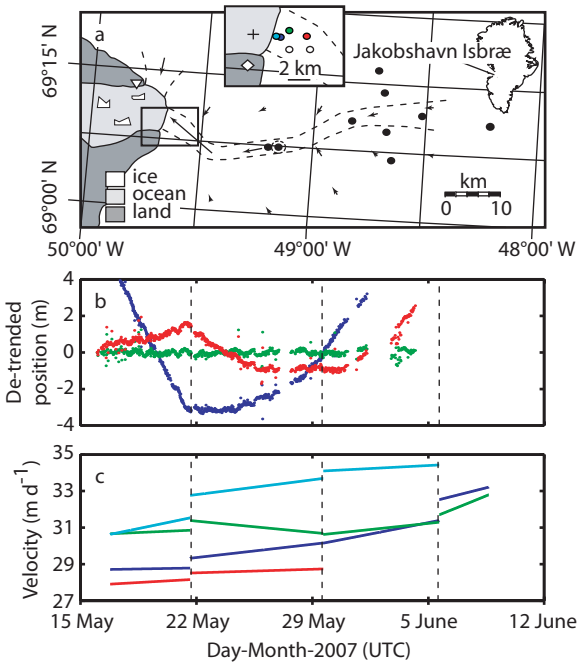

Figure 2.1. Jakobshavn Isbræ and motion surveying data. (a) Map showing locations of the glacier GPS (black circles), iceberg GPS (plus sign), southern (diamond) and northern (triangle) GPS base stations, and optical survey markers (circles in the inset). A seismometer and cameras were located near the southern base station. Arrows roughly indicate the ice flow direction and relative magnitude. Dashed lines mark the margins of fast moving ice. (b) De-trended along-flow positions for the near terminus marker (light blue circle in (a)), assuming constant velocity (blue), constant but non-zero strain rate (red), and strain rates that change at each calving event but otherwise remain constant and non-zero (green). Calving events are indicated by dashed lines. The root mean square errors are 3.06, 0.86, and 0.12 m, respectively. Note the break in slope of the red and blue curves on 21 May. Data gaps are due to bad weather. (c) Velocity of the four fastest survey markers (line colors correspond to markers in (a)).

Jakobshavn Isbræ (Figure 2.1a), which drains 7% of the Greenland Ice Sheet [*Bindschadler*, 1984], began a calving retreat in the 1990's [*Luckman and Murray*, 2005] after roughly 50 years of terminus stability [*Sohn et al.*, 1998]. Initial thinning [*Thomas*, 2004] and acceleration [*Joughin et al.*, 2004] of the glacier has been followed by the collapse of an extensive floating tongue and over 10 km of terminus retreat [*Csatho et al.*, 2008]. The terminus, which now fluctuates ∼5 km annually [double the pre-retreat fluctuations, *Sohn et al.*, 1998], is floating in winter and grounded in late summer. These variations are visible in

time-lapse photography: icebergs calved in summer often contain dirty basal ice and are smaller and more rounded (never tabular) than icebergs calved in winter. Furthermore, surveying measurements (discussed below) show that there is no vertical tidal motion of the terminus in summer. Calving that occurs in summer therefore differs from calving events that occurred prior to the loss of the glacier's extensive floating tongue, which persisted year round and calved tabular icebergs in summer [*Hughes*, 1986]. In this paper we characterize recent large calving events and the glacier, fjord, and seismic response to these events.

2.2 Methods

During summer 2007 we deployed several instruments, all synchronized to UTC time, to study Jakobshavn Isbræ and its proglacial fjord (Figure 2.1a) before, during, and after large calving events. Three cameras took photos of the terminus and fjord every 10 minutes from 13 May to 8 June 2007, every hour from 8 June to 17 August 2007, every six hours from 23 August 2007 to 7 May 2008, and every 10 minutes from 7 May to 14 May 2008. Ocean and seismic waves from calving events were recorded with a tide gauge and a seismometer. A Keller DC-22 pressure sensor, which has a resolution of 0.002 m, was placed in Ilulissat Harbor, 50 km west of the glacier terminus; it logged data every 10 minutes from 11 May to 22 August 2007. A Mark Products L22 3-component velocity seismometer was placed on bedrock 1 km south of the glacier terminus and ran with a sampling frequency of 200 Hz from 17 May to 17 August 2007 and 100 Hz from 22 August to 22 November 2007 and from 9 April to 9 May 2008. The data gap in winter was due to a loss of battery power. The instrument has a natural frequency of 2 Hz and a sensitivity of 88 V s m^{-1}.

Optical and GPS surveys were conducted to monitor iceberg and glacier motion. Six survey reflectors were placed on the lower 4 km of the glacier and surveyed every 15 minutes with a Leica automatic theodolite from 15 May to 9 June 2007. Nine dual-frequency GPS receivers were deployed higher on the glacier, five on the main flow line and four on a perpendicular transect. These units were installed between 22 May and 1 June 2007 and,

except for three that failed in July, ran until 23 August 2007. Additionally, two telemetered GPS units were placed on large icebergs; data from these were retrieved from 29 May to 8 June 2007. All GPS units logged position data every 15 seconds. The data were differentially corrected against one of two base stations located on opposite sides of the fjord. The measurement uncertainties of the optical and GPS surveys were estimated by de-trending several days of data at a time, removing extreme outliers that clearly indicate bad surveys, and calculating the root mean square errors. The errors for the optical and GPS surveys were $\pm$0.15 m and $\pm$0.02 m, respectively.

2.3 Description of Calving Events

We documented 32 large calving events between 13 May 2007 and 14 May 2008 (Table 2.A-1) with time-lapse photography and passive seismology. Seven events, including one in 2006, were directly observed. Twenty-five events occurred between 16 May and 2 August 2007, or at a mean rate of about one every 75 hours. The calving rate greatly decreased in winter: three events occurred between 17 August and 17 October 2007 and no additional events occurred until April 2008. The short floating tongue that developed over winter disintegrated in a sequence of four calving events between 19 April and 10 May 2008.

Hereafter we focus on calving that occurred in summer from a grounded terminus. We observed calving icebergs that penetrated the entire glacier thickness ($\sim$900 m, see below) and were a kilometer in lateral width and several hundred meters in the flow direction (Figure 2.2). The calving events typically lasted 30–60 min, during which several of these icebergs calved and overturned (top toward or away from the terminus). Each iceberg rotated 90° within 5 min (Figure 2.2c–f), displaced up to $\sim$0.5 km^3 of water, and lost more than 10^{14} J of potential energy. As a result the icebergs sprayed water and ice particles over the 100 m high terminus, produced ocean waves with local amplitudes of several meters and periods greater than 30 s (Videos 2.B-1 and 2.B-2), and propelled most icebergs in the ice-choked fjord rapidly down fjord ($\sim$2 km in an hour, Figure 2.A-1). Icebergs near the terminus abruptly decelerated once the events ended (Video 2.B-2). On one occasion (17

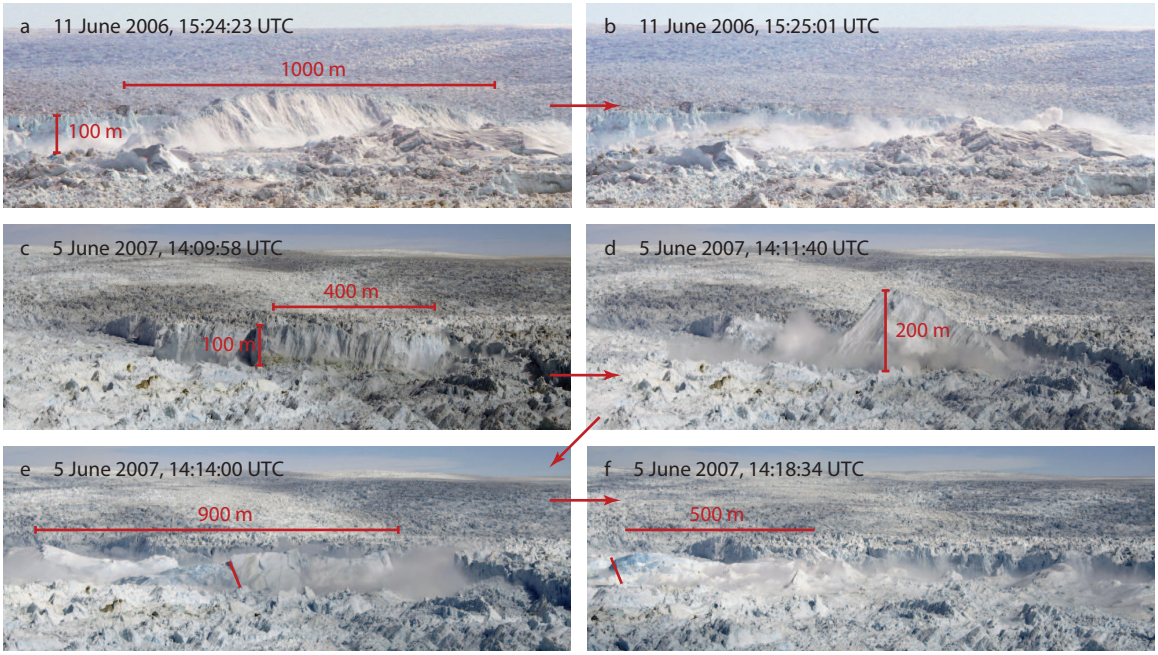

Figure 2.2. Imagery of calving events. (a–b) A calving event on 11 May 2006. Photos were taken from the north side of the fjord. The time stamps may differ from UTC by 1–2 min. (c–f) The third of three calving events on 5 June 2007. Photos were taken from the south side of the fjord. The time stamps are within seconds of UTC. In (f), the arrow represents the distance that the notch in the iceberg (marked in red) traveled between frames (e) and (f).

August 2007) icebergs at the fjord mouth 50 km away were observed moving 1–2 km hr^{-1} several hours after an event. Furthermore, waves from all events were detected by our tide gauge 30 min after calving initiated and for a duration of six hours (with amplitudes much reduced, Figure 2.A-2). Similar waves have been attributed to, but not correlated with, calving [*Sørensen and Schrøder*, 1971]. In contrast, between events icebergs in the upper fjord were pushed forward at the same speed as the advancing terminus ($\sim$35 m d^{-1}, see Figure 2.A-1 and below).

A similar calving event was recently observed at Columbia Glacier, Alaska, as its terminus became buoyant (T. Pfeffer, personal communication, 2008). More commonly, though, large calving events observed at grounded tidewater glaciers in Alaska involve the top, middle, and bottom parts of the termini calving separately and in succession within 5–30

min [*O'Neel et al.*, 2003].

Our local, land-based seismometer recorded unique seismic signals originating from the calving events. The seismograms are characterized by (1) emergent, cigar-shaped envelopes that last about as long as the calving events (up to an hour) and have several peaks, (2) high energy between 0.5 and 30 Hz with maximum energy at ∼4 Hz, (3) ground motion that, at low frequencies, is preferentially-oriented perpendicular to the fjord walls, (4) continuously elevated seismic activity for several hours after calving (sometimes over 24 hours)(Figure 2.3), (5) resemblance to seismograms produced by icebergs overturning in the fjord (Figure 2.A-3) during periods of no calving, and (6) occasionally have one or two high amplitude spikes that document maximum ground motion during the events and contain significant energy below 1 Hz (Figure 2.3c–f). Characteristics (1) and (2) are in good agreement with observations at Columbia Glacier [*Qamar*, 1988; *O'Neel et al.*, 2007]. While these seismograms may be a result of water-driven fracture propagation [*O'Neel et al.*, 2007], characteristics (1) and (3)–(5) suggest that much of the local seismic signal is instead caused by the loading and unloading of the coast by large ocean waves [e.g., *Yuan et al.*, 2005], which may disturb the densely-packed fjord for hours. We propose that the emergent, cigar-shaped envelopes reflect the gradual growth and decay of ocean waves during calving events and the peaks reflect the detachment and overturning of individual icebergs.

Seismograms of glacial earthquakes (discussed below) closely resemble local and far-field seismograms from calving events (Figure 2.A-4). This more tightly-constrains the observation that glacial earthquakes are associated with calving [*Joughin et al.*, 2008]. Not all calving events produce glacial earthquakes and furthermore, glacial earthquakes only occupy short time windows within the locally recorded seismograms (e.g., the spike in Figure 2.3c is a candidate for a glacial earthquake).

In contrast to the activity at the terminus and in the fjord, changes in glacier motion associated with calving were small. At no time before, during, or after calving did any of the glacier survey markers experience jumps in horizontal position larger than the error

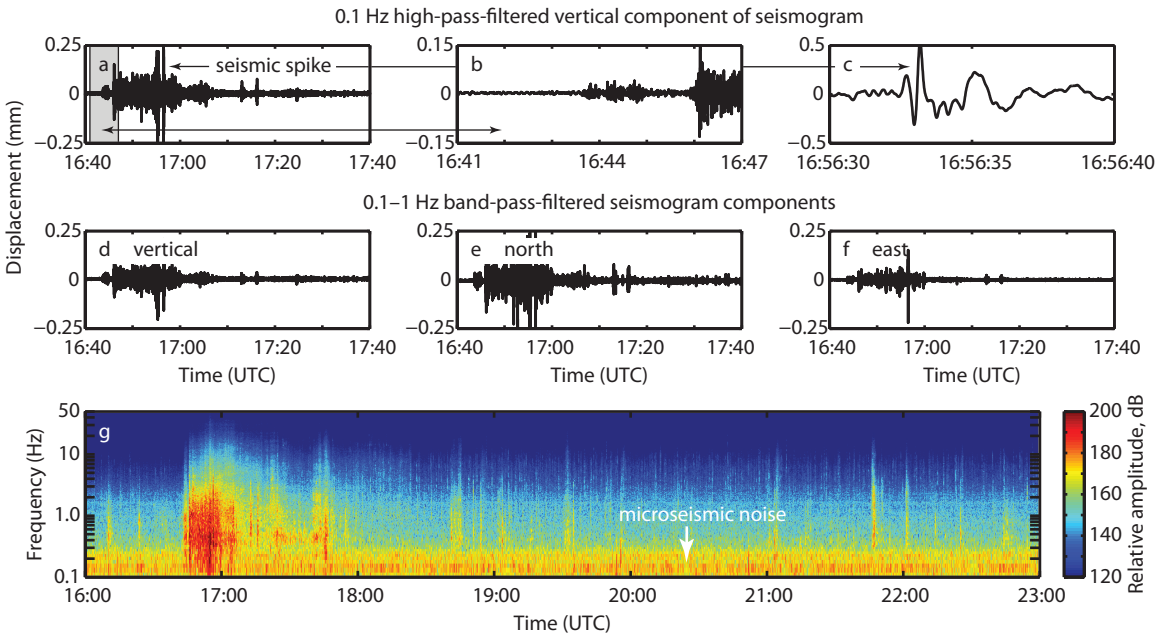

Figure 2.3. Seismogram from the 4 July 2007 calving event. The data were corrected for instrument response and integrated. (a) 0.1 Hz high-pass-filtered vertical seismogram component that had (b) an emergent onset and (c) a high-amplitude seismic spike. (d–f) 0.1–1 Hz band-pass filtered vertical, north, and east seismogram components. The fjord walls run roughly east-west. (g) Spectrogram of the calving event. Note the slightly elevated energy content that lasted for several hours after the calving event.

of the survey measurements ($\pm$0.15 m and $\pm$0.02 m for the near-terminus optical and up-glacier GPS surveys, respectively)(Figures 2.1b, 2.A-5, and 2.A-6). However, the position plots for the near-terminus markers do show breaks in slope, which are indicative of step changes in velocity, that coincide with calving events (Figure 2.1b and 2.A-5). To quantify the step changes, we split the data into intervals bounded by calving events, rotated them into along- and across-flow directions, and assumed that the velocity at fixed points in space remains constant between calving events. Thus, the total derivative of a marker's along-flow velocity within each interval is

$$\frac{Du}{Dt} = \frac{\partial u}{\partial x}\frac{dx}{dt} + \frac{\partial u}{\partial t} = \dot{\varepsilon}_{xx} u, \tag{2.1}$$

where x, u, and $\dot{\varepsilon}_{xx}$ are the along-flow position, velocity, and extensional strain rate, and t

is time. Integrating twice gives

$$x(t) = \frac{u_0}{\dot{\varepsilon}_{xx}} \left[\exp(\dot{\varepsilon}_{xx}(t - t_0)) - 1\right] + x_0. \tag{2.2}$$

x_0, u_0, and $\dot{\varepsilon}_{xx}$ are found for each interval by fitting Equation 2.2 through the position data. The results are used to calculate $u(t)$ (Figure 2.1c).

The glacier velocity was $\sim$35 m d^{-1} near the terminus (Figure 2.1c), decreasing to 20–25 m d^{-1} just 4 km upglacier. During calving events the velocities of the markers increased by $\sim$3% (0.5–1.5 m d^{-1}). Changes were largest for markers located closest to the terminus and were only detectable within 3–4 km of the terminus. The velocity changes were comparable to multiplying the longitudinal strain rate at a survey marker by the amount of terminus retreat from a given calving event. We therefore attribute the velocity changes to the glacier rapidly adjusting its stress field as the terminus (a free boundary) moves up glacier.

2.4 Calving-Induced Glacial Earthquakes

Our surveying data contradicts the hypothesis that teleseismic glacial earthquakes are generated by glaciers sliding several decimeters to several meters within minutes [*Ekström et al.*, 2003, 2006; *Tsai and Ekström*, 2007], possibly in response to calving [*Joughin et al.*, 2008; *Tsai et al.*, 2008]. Such earthquakes are characterized by long period (35–150 s), large magnitude (M_{sw} 4.6–5.1) tremors that originate from the terminal regions of major outlet glaciers in Greenland (including Jakobshavn Isbræ), occur predominantly in summer, have occurred more frequently as the glaciers have retreated [*Ekström et al.*, 2003, 2006; *Tsai and Ekström*, 2007], and appear to be associated with the calving of large, overturning icebergs from grounded termini [*Joughin et al.*, 2008]. Far-field seismic waveforms from the earthquakes can be fit with mass-sliding models using force vectors that are horizontal and parallel to the glacier flow lines [*Ekström et al.*, 2003, 2006; *Tsai and Ekström*, 2007].

We propose the alternative hypothesis, consistent with these and our observations, that glacial earthquakes are generated by icebergs overturning [also proposed by *Tsai et al.*,

2008] and scraping the fjord bottom during calving. Hydrostatic imbalance during overturning greatly increases the energy of a calving iceberg and, furthermore, icebergs that calve from a grounded or nearly-grounded terminus and penetrate the entire glacier thickness must scrape the fjord bottom as they overturn. Our hypothesis is also consistent with the observation that most known glacial earthquakes that originated near Jakobshavn Isbræ occurred as the glacier was retreating past a shallow pinning point [*Luckman and Murray*, 2005; *Tsai and Ekström*, 2007].

The calving icebergs in Figure 2.2 penetrated the entire ice thickness and brought dirt to the fjord surface. Thus they were approximately 900 m thick: the glacier was 1000 m thick in the late 1980's at what is now the terminus [*Clarke and Echelmeyer*, 1996] and has since thinned by 100 m [*Thomas*, 2004]. Furthermore, since the terminus is grounded during summer, the water depth must not exceed about 800 m. Icebergs that are 900 m thick by 400 m along flow (e.g., Figure 2.2c–f) achieve a maximum total vertical dimension of 985 m during overturning; the icebergs can therefore reach $\sim$200 m above sea level by pushing off the fjord bottom during calving. The iceberg in Figure 2.2a–b rotated 45° in 30–40 s; it had a rotational kinetic energy of 5.0–9.0$\times 10^{12}$ J (1000 m wide, 900 m high, 400 m long). For comparison, a tabular iceberg that ran aground in Antarctica had a kinetic energy of 1.1$\times 10^{13}$ J prior to grounding and produced a moderately sized earthquake (M_l 3.6) containing low-frequency tremors ($<$0.5 Hz). The iceberg contained four orders of magnitude more energy than was needed to produce the M_l 3.6 earthquake [*Müller et al.*, 2005]. Thus some calving icebergs contain enough energy to produce glacial earthquakes.

2.5 Conclusions

Calving at Jakobshavn Isbræ involves the detachment and overturning of several large icebergs within 30–60 min, causes most icebergs in the ice-choked fjord to move 2 km in an hour, produces ocean waves that are detectable 50 km away, and emits long-lasting and far-reaching seismic signals. It is now clear that teleseismic glacial earthquakes are generated during calving events, although the specific source mechanism remains unclear

[*Tsai et al.*, 2008]. Despite the large amount of energy released during calving there is little response from the glacier, thus indicating that glacial earthquakes are not caused by episodic rapid glacier slip [e.g., *Ekström et al.*, 2003]. The observations presented here are an important step toward assessing the mechanisms controlling calving at major outlet glaciers in Greenland.

Acknowlegdments

We thank J. Brown and D. Maxwell for field assistance, and S. Anandakrishnan, A. Behar, and R. Fatland for loaning GPS receivers. Comments from editor E. Rignot and reviewers S. O'Neel and T. Pfeffer improved the manuscript. Logistics and instrumental support were provided by VECO Polar Resources, UNAVCO, and PASSCAL. Seismic analysis was done with the Matlab waveform object package written by Celso Reyes (http://www.giseis.alaska.edu/Seis/EQ/tools/matlab/). Funding was provided by NASA's Cryospheric Sciences Program (NNG06GB49G), the U.S. National Science Foundation (ARC0531075), the Swiss National Science Foundation (200021-113503/1), the Comer Science and Education Foundation, and a CIFAR IPY student fellowship under NOAA cooperative agreement NA17RJ1224 with the University of Alaska.

References

Abdalati, W., et al. (2001), Outlet glacier and margin elevation changes: Near-coastal thinning of the Greenland Ice Sheet, *J. Geophys. Res.*, *106*(D24), 33,729–33,741.

Bindschadler, R.A. (1984), Jakobshavns Glacier drainage basin: A balance assessment, *J. Geophys. Res.*, *89*(C2), 2066–2072.

Clarke, T.S., and K. Echelmeyer (1996), Seismic-reflection evidence for a deep subglacial trough beneath Jakobshavn Isbræ, West Greenland, *J. Glaciol.*, *42*(141), 219–232.

Csatho, B., T. Schenk, C.J. van der Veen, and W.B. Krabill (2008), Intermittent thinning of Jakobshavn Isbræ, West Greenland, since the Little Ice Age, *J. Glaciol.*, *54*(184), 131–144.

Ekström, G., M. Nettles, and G.A. Abers (2003), Glacial earthquakes, *Science*, *302*(5645), 622–624, doi:10.1126/science.1088057.

Ekström, G., M. Nettles, and V. Tsai (2006), Seasonality and increasing frequency of glacial earthquakes, *Science*, *311*(5768), 1756–1758, doi:10.1126/science.1122112.

Hughes, T. (1986), The Jakobshavns effect, *Geophys. Res. Lett.*, *13*(1), 46–48.

IPCC (2007), *Climate Change 2007: The Physical Science Basis. Contribution of Working Group I to the Fourth Assessment Report of the Intergovernmental Panel on Climate Change* (Cambridge University Press, Cambridge and New York, 2007), pp. 996.

Joughin, I., W. Abdalati, and M. Fahnestock (2004), Large fluctuations in speed on Greenland's Jakobshavn Isbræ glacier, *Nature*, *432*, 608–610, doi:10.1038/nature03130.

Joughin, I., I. Howat, R.B. Alley, G. Ekström, M. Fahnestock, T. Moon, M. Nettles, M. Truffer, and V. C. Tsai (2008), Ice-front variation and tidewater behavior on Helheim and Kangerdlugssuaq Glaciers, Greenland, *J. Geophys. Res.*, *113*, F01004, doi:10.1029/2007JF000837.

Luckman, A., and T. Murray (2005), Seasonal variation in velocity before retreat of Jakobshavn Isbræ, Greenland, *Geophys. Res. Lett.*, *32*, L08501, doi:10.1029/2005GL022519.

Müller, C., V. Schlindwein, A. Eckstaller, H. Miller (2005), Singing icebergs, *Science*, *310*(5752), 1299, doi:10.1126/science.1117145.

O'Neel, S., K.A. Echelmeyer, and R.J. Motyka (2003), Short-term variations in calving of a tidewater glacier: LeConte Glacier, Alaska, U.S.A., *J. Glaciol.*, *49*(167), 587–598.

O'Neel, S., H.P. Marshall, D.E. McNamara, and W.T. Pfeffer (2007), Seismic detection and analysis of icequakes at Columbia Glacier, Alaska, *J. Geophys. Res.*, *112*(F03S23), doi:10.1029/2006JF000595.

Qamar, A. (1998), Calving icebergs: A source of low-frequency seismic signals from Columbia Glacier, Alaska, *J. Geophys. Res.*, *93*(B6), 6615–6623.

Rahmstorf, S. (2007), A semi-empirical approach to projecting future sea-level rise, *Science*, *315*(5810), 368–370, doi:10.1126/science.1135456.

Rignot, E. and P. Kanagaratnam (2006), Changes in the velocity structure of the Greenland Ice Sheet, *Science*, *311*(5763), 986–990, doi:10.1126/science.1121381.

Sørensen, T. and H. Schrøder (1971), Long period wave phenomena in Jakobshavn Harbour Bay, Greenland, *Proceedings from the First International Conference on Port and Ocean Engineering under Arctic Conditions 2*, 1312–1324.

Sohn, H.G., K.C. Jezek, and C.J. van der Veen (1998), Jakobshavn Glacier, West Greenland: 30 years of spaceborne observations, *Geophys. Res. Lett.*, *25*(14), 2699–2702.

Thomas, R.H. (2004), Force-perturbation analysis of recent thinning and acceleration of Jakobshavn Isbræ, Greenland, *J. Glaciol.*, *50*(168), 57–66.

Tsai, V.C. and G. Ekström (2007), Analysis of glacial earthquakes, *J. Geophys. Res.*, *112*(F03S22), doi:10.1029/2006JF000596.

Tsai, V.C., J.R. Rice, and M. Fahnestock (2008), Possible mechanisms for glacial earthquakes, *J. Geophys. Res.–Earth Surfaces*, *113*(F03014), doi:10.1029/2007JF000944.

Yuan, X., R. Kind, and H.A. Pedersen (2005), Seismic monitoring of the Indian Ocean tsunami, *Geophys. Res. Lett.*, *32*(L15308), doi:10.1029/2005GL023464.

Appendix 2.A

Table 2.A-1: List of all recorded calving events and associated seismograms (UTC time) from Jakobshavn Isbrae between 13 May 2007 and 14 May 2008. One photo was taken every 10 minutes from 13 May to 9 June 2007 and from 7 May to 14 May 2008, every hour from 9 June to 17 August 2007, and every six hours from 23 August 2007 to 15 March 2008. No photos were taken between 17–23 August 2007. The time given refers to the last photo taken prior to there being any noticeable calving. The seismograms are highly emergent, so the onset times should be used with caution. The seismicity on 18 May 2007 was generated by an iceberg overturning during a period of no calving (Figure S3). Times were not given for the photos of the 19 September 2007 and 17 October 2007 events as they could only be photographically constrained to within 24 hours. * indicates events that were observed and photographed in person.

Date	Time of Photo	Seismogram Onset
*16 May 2007	19:29:31	null
*18 May 2007	09:49:33	09:51:40
21 May 2007	null	16:32:36
29 May 2007	13:59:48	14:04:32
*5 June 2007	09:09:58	09:11:07
*5 June 2007	13:09:58	13:07:42
*5 June 2007	13:59:58	14:07:44
20 June 2007	05:00:20	05:30:00
27 June 2007	15:00:31	15:05:04
29 June 2007	05:00:34	05:49:30
30 June 2007	null	10:41:48
3 July 2007	20:00:40	20:37:48
4 July 2007	06:00:40	06:46:54
4 July 2007	16:00:41	16:43:35
10 July 2007	07:00:49	07:52:00
14 July 2007	07:00:55	07:38:05
16 July 2007	10:00:58	10:34:05

Continued on next page

Date	Time of Photo	Seismogram Onset
16 July 2007	15:00:58	15:21:43
17 July 2007	15:00:59	15:29:47
26 July 2007	18:01:12	18:22:02
30 July 2007	11:01:17	11:25:22
30 July 2007	19:01:18	18:49:29
1 August 2007	20:01:21	19:51:43
2 August 2007	13:01:22	13:31:31
2 August 2007	19:01:22	19:02:54
*17 August 2007	12:01:43	null
19 September 2007	null	06:16:56
17 October 2007	null	08:49:01
19 April 2008	null	15:39:48
26 April 2008	null	11:58:01
3 May 2008	09:24:04	09:49:00
*10 May 2008	21:01:50	21:00:12

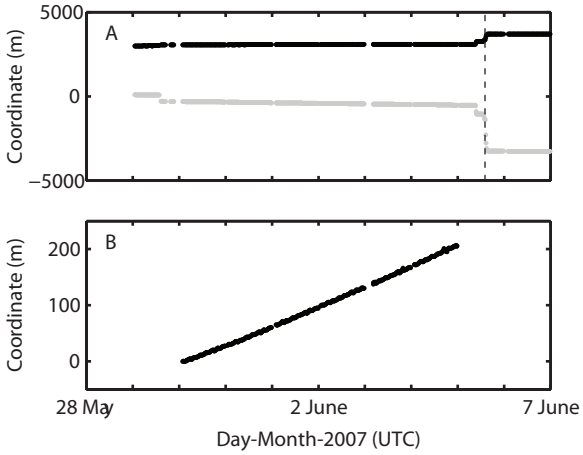

Figure 2.A-1. Iceberg motion recorded with a GPS. The dotted line indicates the timing of a calving event. (a) Northing (black) and easting (gray) of the iceberg relative to the southern GPS base station. (b) Flow line coordinates for the time period preceding the calving event. A least-squares regression to this line gives a mean velocity of about 35 m $a^{-}1$.

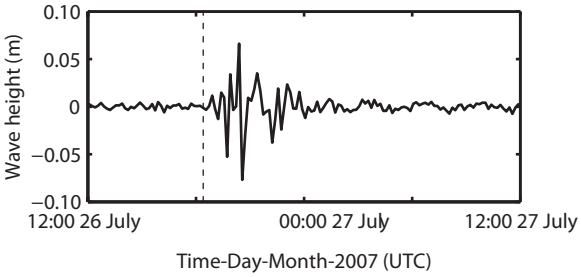

Figure 2.A-2. Example of a wave in Ilulissat Harbor, near the fjord mouth, that was produced by a calving event (dotted line). The plot was generated by running a 3-hr high pass filter on the tide data.

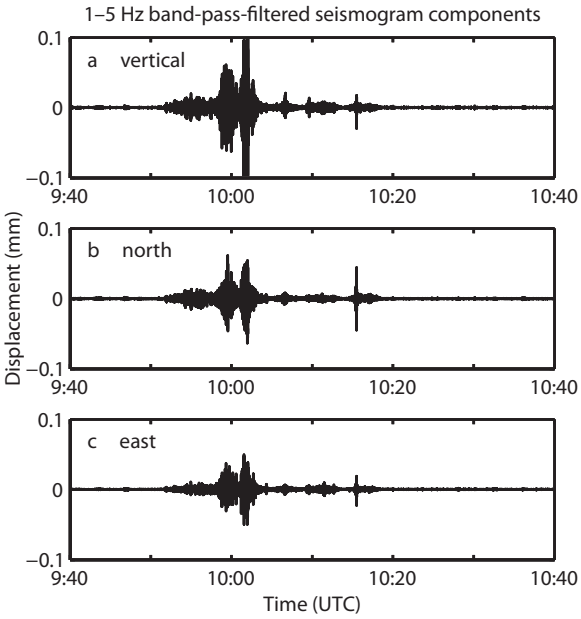

Figure 2.A-3. Seismogram generated by the overturning of a large iceberg on 18 May 2007 during a period of no calving. The data was corrected for instrument response and passed through a 1–5 Hz band-pass filter. (a–c) Vertical, north, and east components, respectively.

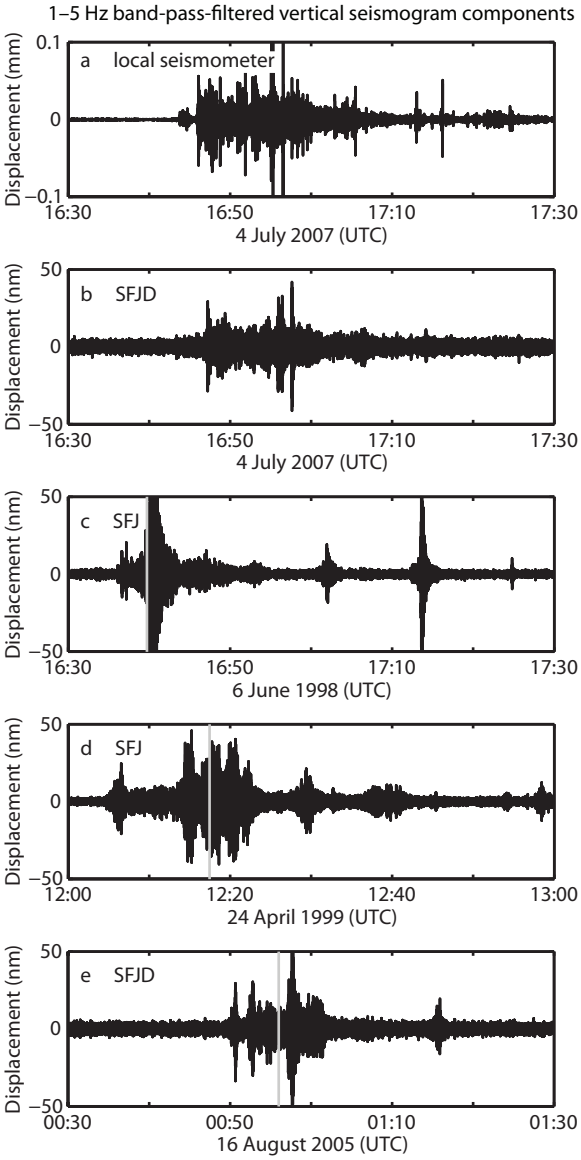

Figure 2.A-4. Comparison of seismograms recorded during a calving event to those recorded during known teleseismic glacial earthquakes. All seismograms have been filtered with a 1–5 Hz band-pass filter. (a) Locally recorded seismogram during the 4 July 2007 calving event. This signal was corrected for instrument response. (b) Seismogram recorded at Global Seismic Network (GSN) station SFJD during the same event as in (a). SFJD is located 250 km south of the glacier terminus. (c–e) Seismograms recorded at GSN stations SFJD and SFJ (SFJ was replaced by SFJD in 2005) during known teleseismic glacial eartquakes that originated from the terminal region of Jakobshavn Isbrae. The gray lines indicate the estimated onset times of the glacial earthquakes [*Tsai and Ekström*, 2007].

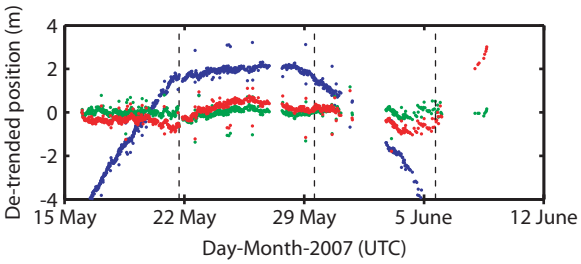

Figure 2.A-5. Glacier motion at one of the optical survey markers (dark blue circle in Figure 1a). The various lines assume constant velocity (blue), constant but non-zero strain rate (red), and strain rates that change at each calving event but otherwise remain constant and non-zero (green). The root mean square errors are 2.49, 0.47, and 0.15 m, respectively. Note the distinct break in slope of the blue and red curves on 21 May. Data gaps are due to bad weather.

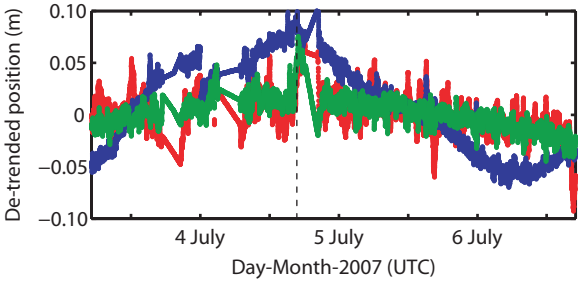

Figure 2.A-6. Glacier motion at one of the GPS sites (the circled block dot in Figure 1a). De-trended longitudinal (blue), transverse (green), and vertical (red) positions. The 4 July 2007 calving event is indicated with a dotted line.

Appendix 2.B

The following supplementary videos are included in a DVD at the end of the thesis.

Video 2.B-1: Time-lapse video of a calving event at Jakobshavn Isbrae on 5 June 2007. The video runs from 14:10–14:28 UTC. Photos were taken every 10 seconds.

Video 2.B-2: Time-lapse video of a calving event at Jakobshavn Isbrae on 17 August 2007. The video runs from 12:42–13:21 UTC. Photos were taken every 5 seconds.

Chapter 3
Ice mélange dynamics and implications for terminus stability, Jakobshavn Isbræ, Greenland [1]

Abstract

We used timelapse imagery, seismic and audio recordings, iceberg and glacier velocities, ocean wave measurements, and simple theoretical considerations to investigate the interactions between Jakobshavn Isbræ and its proglacial ice mélange. The mélange behaves as a weak, granular ice shelf whose rheology varies seasonally. Sea ice growth in winter stiffens the mélange matrix by binding iceberg clasts together, ultimately preventing the calving of full-glacier-thickness icebergs (the dominant style of calving) and enabling a several kilometer terminus advance. Each summer the mélange weakens and the terminus retreats. The mélange remains strong enough, however, to be largely unaffected by ocean currents (except during calving events) and to influence the timing and sequence of calving events. Furthermore, motion of the mélange is highly episodic: between calving events, including the entire winter, it is pushed down fjord by the advancing terminus (at $\sim$40 m d^{-1}), whereas during calving events it can move in excess of 50×10^3 m d^{-1} for more than 10 min. By influencing the timing of calving events, the mélange contributes to the glacier's several-kilometer seasonal advance and retreat; the associated geometric changes of the terminus area affect glacier flow. Furthermore, a force balance analysis shows that large-scale calving is only possible from a terminus that is near floatation, especially in the presence of a resistive ice mélange. The net annual retreat of the glacier is therefore limited by its proximity to floatation, potentially providing a physical mechanism for a previously described near-floatation criterion for calving.

[1]Published as Amundson, J.M, M. Fahnestock, M. Truffer, J. Brown, M.P. Lüthi, and R.J. Motyka, 2010. Ice mélange dynamics and implications for terminus stability, Jakobshavn Isbræ, Greenland. *J. Geophys. Res.*, *115*(F01005), doi:1029/2009JF001405.

3.1 Introduction

The recent thinning [*Thomas et al.*, 2000; *Abdalati et al.*, 2001; *Krabill et al.*, 2004], acceleration [*Joughin et al.*, 2004; *Howat et al.*, 2005; *Luckman et al.*, 2006; *Rignot and Kanagaratnam*, 2006], and retreat [*Moon and Joughin*, 2008; *Csatho et al.*, 2008] of outlet glaciers around Greenland has stimulated a discussion of the processes controlling the stability of the Greenland Ice Sheet. These rapid changes are well correlated with changes in ocean temperatures both at depth [*Holland et al.*, 2008] and at the surface [*Howat et al.*, 2008]. Furthermore, velocity variations on these fast flowing outlet glaciers appear to be linked to changes in glacier length and are largely unaffected by variations in surface melt rates [*Joughin et al.*, 2008b]. Thus, the observed changes in glacier dynamics and iceberg calving rates are likely driven by processes acting at the glacier-ocean interface.

Large calving retreats at some glaciers have been correlated with the loss of buttressing sea ice [e.g., *Higgins*, 1991; *Reeh et al.*, 2001; *Copland et al.*, 2007]. Likewise, the seasonal advance and retreat of Jakobshavn Isbræ (Fig. 3.1)(Greenlandic name: Sermeq Kujalleq), one of Greenland's largest and fastest-flowing outlet glaciers, is well-correlated with the growth and decay of sea ice in the proglacial fjord [*Birnie and Williams*, 1985; *Sohn et al.*, 1998; *Joughin et al.*, 2008c]. It therefore appears that sea ice, despite being relatively thin, may help to temporarily stabilize the termini of tidewater glaciers.

Presently, calving ceases at Jakobshavn Isbræ in winter, causing the terminus to advance several kilometers and develop a short floating tongue [*Joughin et al.*, 2008b; *Amundson et al.*, 2008]. The newly-formed tongue rapidly disintegrates in spring after the sea ice has retreated to within a few kilometers (or less) of the terminus [*Joughin et al.*, 2008c] and before significant surface melting has occurred. The rapid disintegration of the newly-formed tongue, which occurs over a period of a few weeks, suggests that the tongue is little more than an agglomeration of ice blocks that are prevented from calving by sea ice and ice mélange (a dense pack of calved icebergs). (Note that we prefer the term ice mélange over the Greenlandic word "sikkusak" [as used in *Joughin et al.*, 2008c], as observations presented here may be applicable to non-Greenlandic glaciers, such as to the Wilkins Ice

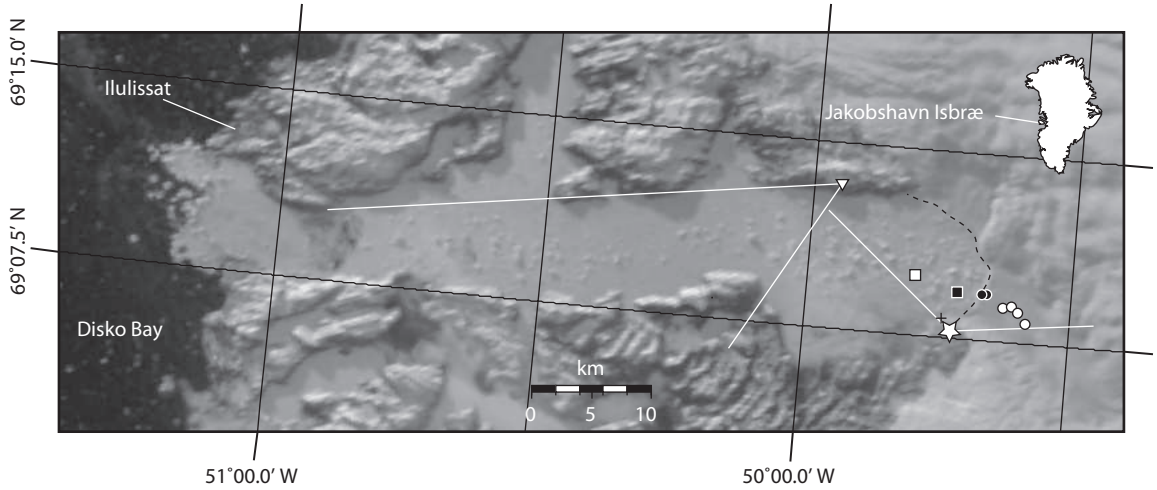

Figure 3.1. MODIS image of the terminal region of Jakobshavn Isbræ and proglacial fjord from 26 May 2007 (day of year 146). The terminus is marked with a dashed line. The seismometer, audio recorder, GPS base station, and one to six timelapse cameras were located near our camp, indicated by a star. An additional camera was placed on the north side of the fjord (triangle) and pointed in the down-fjord direction. The approximate field of view of the cameras is indicated by the white lines. Also indicated are the initial positions of the 2007 (black circles) and 2008 (white circles) surveying prisms used in Figure 3.3, the initial positions of the 2007 (black square) and 2008 (white square) iceberg GPS receivers, and the pressure sensor (small cross) that was used to measure ocean waves.

Shelf during its recent disintegration [e.g., *Scambos et al.*, 2009; *Braun et al.*, 2009].)

Visual observations of Jakobshavn Isbræ's proglacial ice mélange suggest that (1) the mélange forms a semi-rigid, visco-elastic cap over the innermost 15–20 km of the fjord, (2) motion of the mélange is primarily accomodated by deformation and/or slip in narrow shear bands within and along the margins of the mélange, and (3) icebergs within the mélange gradually disperse and become isolated from each other as they move down fjord. We propose that the mélange is essentially a weak, poorly-sorted, granular ice shelf, and is therefore capable of influencing glacier behavior by exerting back pressure on the glacier terminus [*Thomas*, 1979; *Geirsdóttir et al.*, 2008]. When shear stresses within the mélange exceed some critical value, the mélange fails along discrete shear margins. Sea ice formation in winter stiffens the mélange matrix and promotes the binding of clasts (icebergs and

larger brash ice components), thereby increasing the mélange's critical shear stress. Thus, sea ice and ice mélange may act together to influence glacier and terminus dynamics.

Here, we use a suite of observations and simple theoretical considerations to investigate the dynamics of Jakobshavn Isbræ's ice mélange and possible mechanisms by which the mélange may influence glacier behavior. Our results have implications for fjord and glacier dynamics, the sequence and timing of calving events, and limitations on the glacier's rate of retreat.

3.2 Methods

Observations in this paper are based on measurements made at Jakobshavn Isbræ (Fig. 3.1) from May 2007 to August 2008. Data collection included several timelapse cameras pointed at the glacier and fjord, optical and GPS surveys of glacier and iceberg motion, a pressure sensor for measuring ocean waves, a seismometer, and an audio recorder. All instruments recorded in UTC.

Anywhere from one to six timelapse cameras were pointed at the terminus and inner fjord between 13 May 2007 and 3 August 2008. The camera systems consisted of a variety of Canon digital cameras, Canon timers, and custom-built power supplies. Four of the cameras were used to capture the seasonal evolution of the glacier's terminus position, which varies ∼5 km over the course of a year [*Joughin et al.*, 2008c; *Amundson et al.*, 2008]. The photo interval for these cameras ranged from 10 min to 6 hr, depending on data storage capacity and the amount of time between field campaigns. The other two cameras took photos of the terminus every 10 s during two field campaigns (from 8–12 May 2008 and from 9–25 July 2008) to capture the full sequence of calving events; they captured nine events before failing. One additional camera was placed ∼10 km down fjord from the terminus and pointed in the down fjord direction; it took photos every hour from 16 May to 9 July 2008 and every 15 min from 9 July to 6 August 2008. During our field campaigns all camera clocks were occasionally checked to correct for clock drift.

Optical surveying prisms were deployed on the lower 4 km of the glacier in both 2007

(7 prisms) and 2008 (10 prisms). The prisms were surveyed with a Leica TM1800 automatic theodolite and DS3000I Distomat every 10–15 min, weather permitting, from 15 May to 9 June 2007 and from 12 July to 4 August 2008. In 2007 five prisms lasted more than 18 days, three of which lasted the entire field campaign. In 2008 one prism lasted the entire field campaign and another lasted 17 days; all others fell over or calved into the ocean within nine days of deployment. The error in the surveyed positions was estimated to be ± 0.15 m [*Amundson et al.*, 2008]. The position data were smoothed with a smoothing spline (using the curve fitting toolbox in MATLAB) and differentiated to calculate velocities. Errors in the velocity calculations are not easily estimated, though we can provide bounds over various time intervals: 0.21 m d^{-1} for daily average velocities, and 0.85 m d^{-1} for 6-hour average velocities.

Iceberg motion was measured with custom built L1-only GPS receivers that were designed for rapid deployment from a hovering helicopter. In 2007 we used a Vexcel microserver ("brick"; http://robfatland.net/seamonster/index.php?title=Vexcel_Microservers). The microserver was connected to a wireless transmitter, enabling data retrieval from camp. In 2008 we used a similar, custom-built 1 W receiver.

GPS data from both years were broken into 15 min intervals and processed as static surveys against a base station at camp. During some periods, such as when the icebergs were moving quickly, we also processed the data using Natural Resources Canada's precise point positioning tool in kinematic mode. The positional uncertainty, determined by calculating the standard deviation of a de-trended section of data, was typically around 1.0 m regardless of whether the data were processed as static or kinematic surveys. As with the optical surveying data (above), the position data were smoothed with a smoothing spline and differentiated to calculate velocities. Error bounds are 1.4 m d^{-1} for daily average velocities, and 5.7 m d^{-1} for 6-hour average velocities.

Ocean stage was measured every 5 s from 15–24 July 2008 with a Global Water water-level sensor (model WL400) that recorded to a Campbell Scientific CR10X datalogger. The sensor had a range of 18.3 m; its output was digitized to a resolution of 4×10^{-3} m. The

instrument was placed in a small tide pool roughly 3 km from the glacier terminus; it was not rigidly attached to the ocean bottom but was weighted with ∼5 kg of rocks.

A Mark Products L22 3-component velocity seismometer was deployed on bedrock south of the terminus. The instrument has a natural frequency of 2 Hz and a sensitivity of 88 V s m^{-1}. The data were sampled with a Quanterra Q330 datalogger and baler. The sample frequency was 200 Hz from 17 May–17 August 2007 and 10 May–3 August 2008, and 100 Hz from 22 August 2007–9 May 2008.

Audio signals were recorded in stereo with two Sennheiser ME-62 omnidirectional condenser microphones separated by 50 m; stereo recording enabled determination of the instrument to source direction. The microphones were powered by Sennheiser K6 power modules and connected to a Tascam HD-P2 stereo audio recorder with Audio Technica XLR microphone cables. The frequency response of the microphones ranges from 20 Hz–20 kHz and is flat up to 5 kHz. Rycote softie windshields were used to reduce wind noise; they have virtually no effect on signals with frequencies higher than ∼400 Hz but cause a 30 dB reduction in signals with frequencies lower than ∼80 Hz. The recorder gain was set at 8 (out of 10); it logged with a sample frequency of 44.1 kHz and recorded WAV (waveform audio format) files to 8-GB compact flash cards. The flash cards were swapped every 12 hours. The time was recorded when starting and stopping the 12 hour sessions; we estimate that the instrument time was always within 2 s of UTC. Nearly continuous recordings were made from 8–14 May 2008 and 13 July–2 August 2008.

3.3 Results

3.3.1 Temporal Variations in Terminus and Ice Mélange Dynamics

The behavior of Jakobshavn Isbræ's ice mélange is highly seasonal and tightly linked to terminus dynamics. In winter, calving ceases, the terminus advances and develops a short floating tongue, and the mélange and newly-formed sea ice are pushed down fjord as a cohesive unit at the speed of the advancing terminus [see also *Joughin et al.*, 2008c]. The mélange strengthens sufficiently to inhibit the overturning of unstable icebergs and fur-

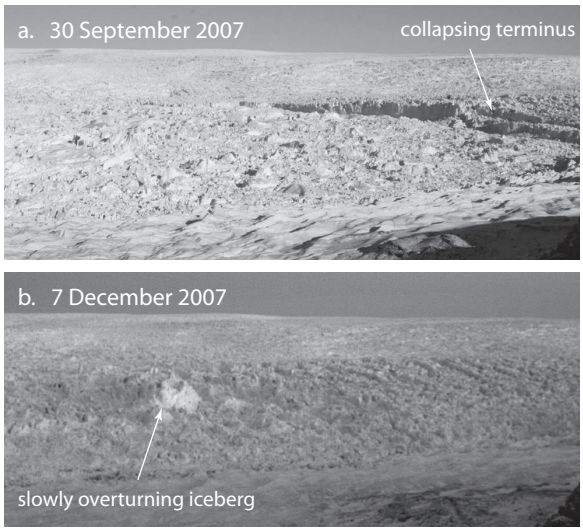

Figure 3.2. Timelapse imagery of the ice mélange. (a) In late September 2007 the terminus began to collapse but was unable to push the mélange out of the way. The slump was present until a calving event on 17 October 2007. (b) A large iceberg in the mélange began overturning on 27 November 2007 and slowly rotated over the course of more than three weeks. Note the smooth transition between ice mélange and floating tongue.

thermore, the floating tongue and ice mélange become nearly indistinguishable in time-lapse imagery (Fig. 3.2). The terminus becomes clearly identifiable only after the floating tongue disintegrates in spring.

Motion of the ice mélange is highly episodic in summer [Video 3.A-1; see also *Birnie and Williams*, 1985; *Amundson et al.*, 2008]. Between calving events the mélange moves down fjord at roughly the speed of the advancing terminus ($\sim$40 m d^{-1}). One to two days prior to a calving event the mélange and lowest-most reaches of the glacier can accelerate up to $\sim$60 m d^{-1} (Fig. 3.3a–b). This acceleration results in 10–20 m of additional displacement and could be due to rift expansion a short distance up-glacier from the terminus. At the onset of a calving event the entire lateral width of the mélange rapidly accelerates away from the terminus, even if the event onset only involves a small portion of the terminus (Videos 3.A-2–3.A-4). Rapid acceleration of the mélange away from the terminus does not appear to precede calving (Fig. 3.3c). During a calving event the mélange can reach speeds greater than 50×10^3 m d^{-1} and extend longitudinally. Once calving ceases, frictional forces

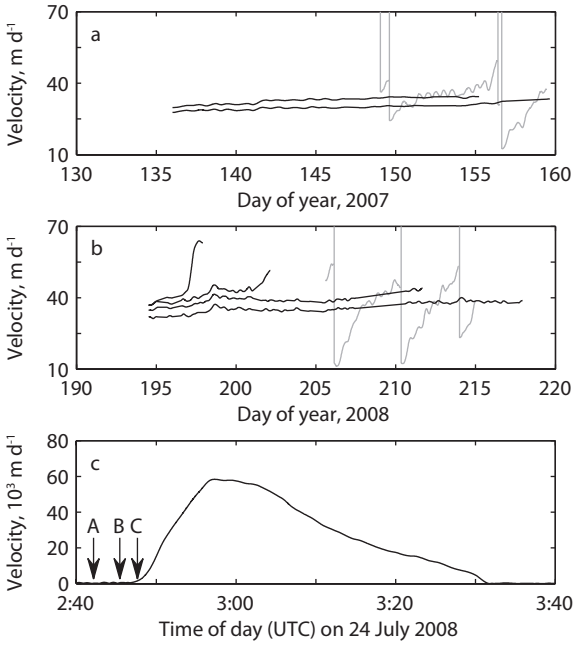

Figure 3.3. Measurements of iceberg and glacier motion. Velocity of an iceberg (gray) and of survey markers on the lower reaches of the glacier (black) during (a) summer 2007 and (b) summer 2008. The large jumps in iceberg velocity are coincident with calving events. The survey markers on the glacier accelerate as they approach the terminus and are eventually calved into the ocean. (c) Iceberg velocity during a calving event on 24 July 2008 (day of year 206; see video 3.A-4). A, B, and C signify the onset of the calving-generated seismogram, the first evidence of activity in the fjord (a small iceberg close to the terminus collapsed), and the first sign of horizontal acceleration of the mélange away from the terminus, as seen in the timelapse imagery.

within the mélange and along the fjord walls cause the mélange to decelerate to roughly one-half of the terminus velocity in ∼30 minutes. Over the next several days the mélange gradually re-accelerates until reaching the speed of the advancing terminus.

In addition to the overall velocity variability described above, the mélange also experiences tidally-modulated, semi-diurnal variations in velocity with an amplitude of ∼4% of the background velocity. No vertical or horizontal tidal signals were observed on the glacier, indicating that the terminus is grounded in summer.

3.3.2 Glaciogenic Ocean Waves

In addition to the rapid horizontal displacement of the ice mélange during calving events, ocean waves generated by calving icebergs cause the mélange to experience meters-scale vertical oscillations. Calving-generated waves can have amplitudes exceeding 1 m at a distance of $\sim$3 km from the terminus with dominant periods of 30–60 s (frequencies of 0.0017–0.033 Hz) (Fig. 3.4a–b; waves can also be seen in Videos 3.A-2–3.A-4). Waves exceeding 1 m amplitude caused the pressure sensor, which was not rigidly attached to the sea floor, to move about in the water column. We are therefore unable to put a reliable upper bound on the size of the ocean waves. We note, though, that waves from one calving event tossed the sensor onto shore from a depth of 10 m. Furthermore, in the vicinity of the terminus, icebergs have been observed to experience vertical oscillations on the order of 10 m during calving events [*Lüthi et al.*, 2009].

Large calving events can also generate lower frequency waves, with spectral peaks at 150 s and 1600 s (0.007 Hz and 6×10^{-4} Hz, respectively). These peaks likely represent eigenmodes (seiches) of the fjord; for example, the shallow water approximation predicts that the fundamental seiche period [e.g., *Dean and Dalrymple*, 1991] is 1250 s for a fjord that is $\sim$0.8 km deep [*Holland et al.*, 2008; *Amundson et al.*, 2008] and 55 km long. The long-period (1600 s) seiche generated on 19 July 2008 had a maximum amplitude of 0.035 m at the site of our pressure sensor, lasted over 8 hours, and decayed with an e-folding time of roughly 3 hrs (Fig. 3.4c). Given our limited observations, it is unclear whether these values are typical. Seiches from the calving events are also recorded in Ilulissat Harbor, over 50 km from the glacier terminus [Fig. 3.A-2 in *Amundson et al.*, 2008]; similar waves have been recorded at Helheim Glacier in East Greenland [*Nettles et al.*, 2008].

3.3.3 Seismic and Acoustic Signals Emanating from the Fjord

Three main types of seismic signals were recorded by the seismometer: (I) impulsive signals with durations of 1–5 s and dominant frequencies of 6–9 Hz (Fig. 3.5a–b), (II) emergent signals with durations of 5–300 s and dominant frequencies of 4–6 Hz (Fig. 3.5c–d), and

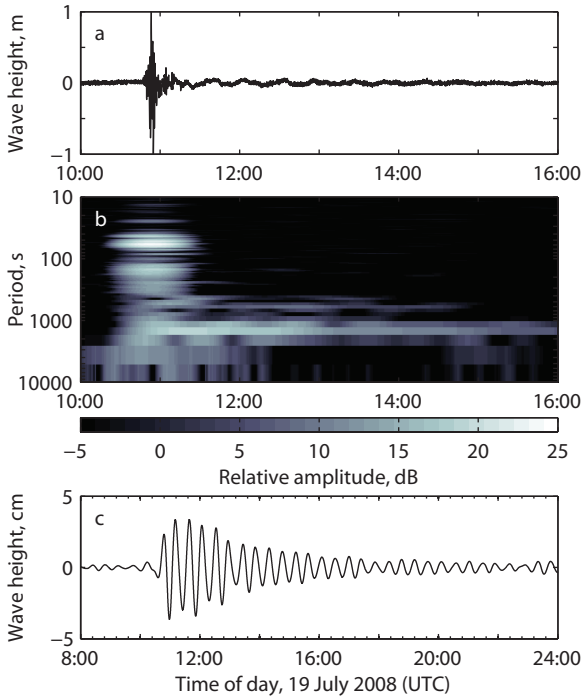

Figure 3.4. Ocean waves produced by a calving event on 19 July 2008. (a) Ocean stage during the calving event after filtering with a 7200-s high-pass filter to remove tidal signals. (b) Spectrogram of the ocean stage showing three spectral peaks. (c) 1000–2000 s band-pass filtered component of the wave; note the different scale of the x- and y-axes.

(III) long-lasting (5–60 min), emergent, high amplitude signals generated by calving icebergs (Fig. 3.6a) and by icebergs overturning during periods of quiescence at the terminus. The general characteristics of the type III signals were discussed in *Amundson et al.* [2008]; we expand on those observations in Section 3.4 with special attention paid to the event onsets and to the proportion of the seismograms that are attributable to motion of the ice mélange.

The occurrence rate of type I and II signals (combined) was determined with a short term averaging / long term averaging (STA/LTA) detector after band-pass filtering the seismic data between 4 and 15 Hz. The STA/LTA ratio was computed using 0.2 s and 30 s windows, respectively, and events were triggered when the ratio exceeded 5. These values were chosen so as to detect both type I and II signals. Changing the detection

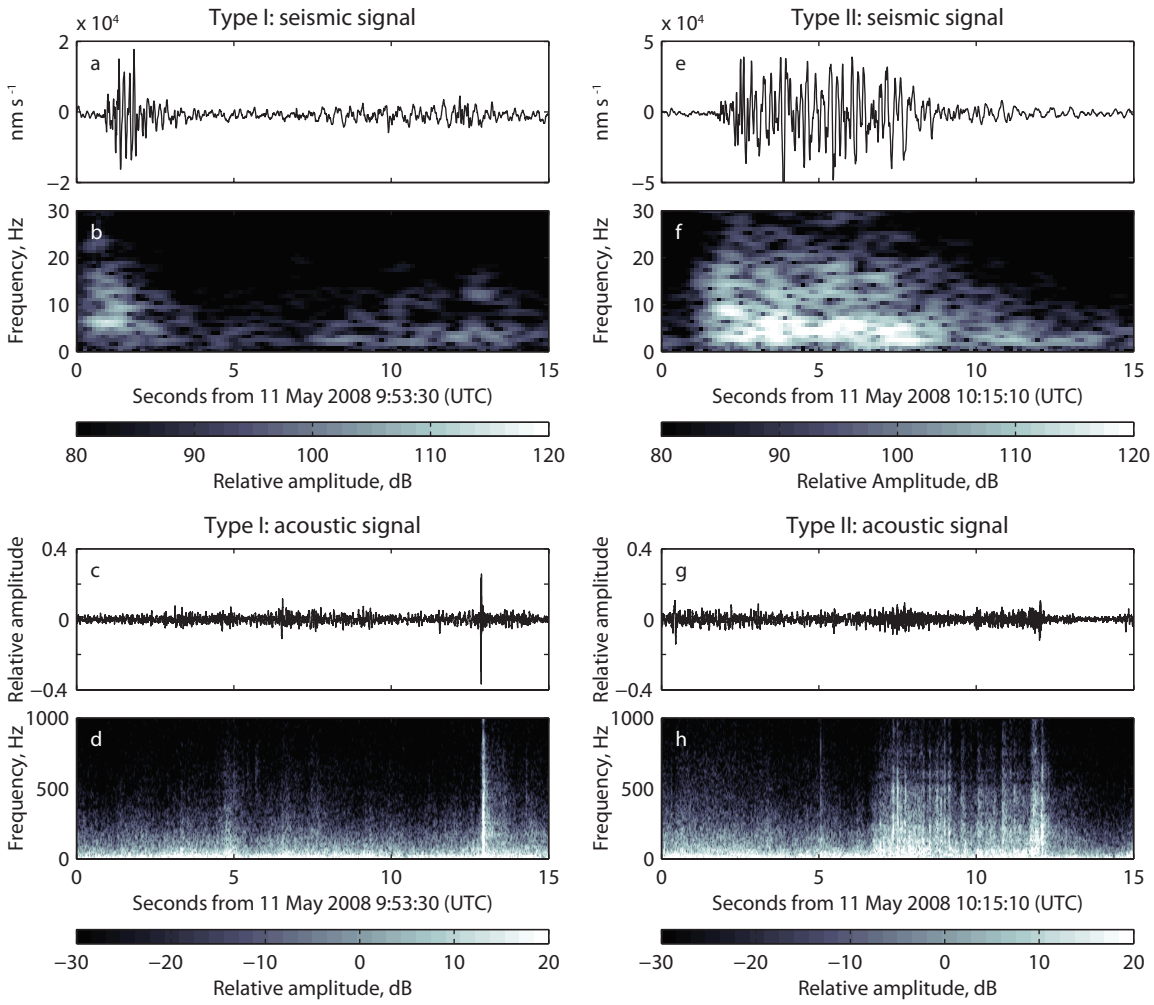

Figure 3.5. Examples of seismic signals originating in the fjord and terminus area. Type I seismic signal and spectrogram ((a)–(b)) and associated acoustic signal ((c)–(d)). Type II seismic signal and spectrogram ((e)–(f)) and associated acoustic signal ((g)–(h)).

parameters affected the total number of detections but did not affect the overall temporal variability. Type I and II signals can occur over 50 times per hour, with greatest activity during and immediately following calving events. On the hourly time scale, there is no obvious change in the number of events immediately preceding a calving event. Between calving events the occurrence rate can decay to less than 10 per hour; the decay occurs with an e-folding time of roughly 12 hr (Fig. 3.7).

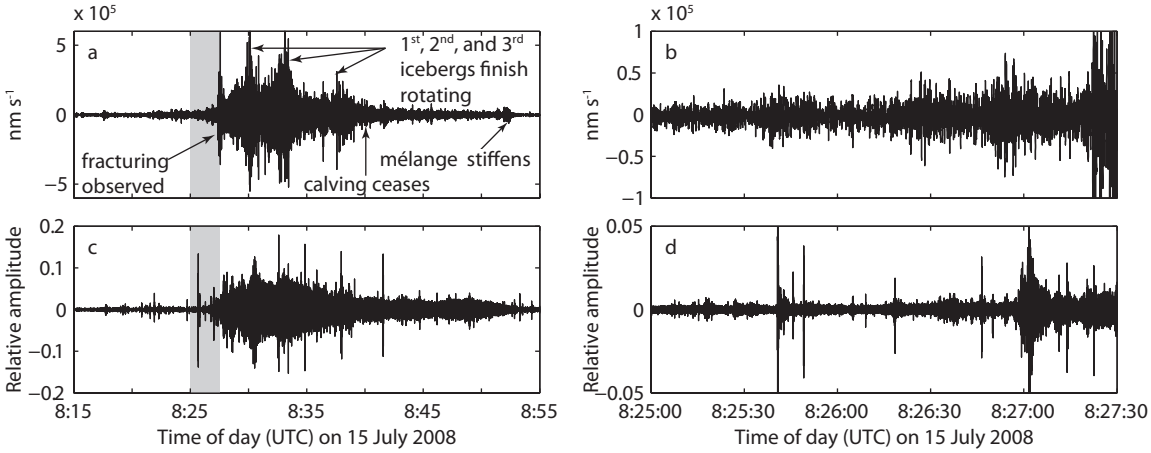

Figure 3.6. Seismic and acoustic waveforms from a calving event on 15 July 2008 (see also Video 3.A-3). (a) Vertical component of the calving-generated seismogram. (b) A close-up of (a) showing the emergent onset of the seismic signal. (c) Acoustic waveform from the calving event. (d) A close-up of (c). The gray panels in (a) and (c) indicate the time periods shown in (b) and (d).

When ambient acoustic noise levels (especially from wind) are low, many of the above-described seismic recordings are easily correlated with acoustic signals. Type I signals are associated with sharp cracking sounds ("shotgun blasts") suggestive of fracturing ice, whereas type II signals are associated with long, low rumblings indicative of avalanching ice debris. These acoustic signals contain significant energy at frequencies ranging from infrasonic ($<$ 20 Hz) to greater than 1 kHz (Fig. 3.5). Stereo recordings of the acoustic signals indicate that they originate at the terminus and from down fjord at roughly equal rates. Calving-generated seismic signals (type III) are associated with both cracking and rumbling sounds (Fig. 3.6a,c).

3.4 Discussion of Calving Events

The general characteristics of calving events and calving-generated seismograms at Jakobshavn Isbræ have been described in *Amundson et al.* [2008]. Here, we expand on those observations by comparing seismograms with audio recordings and high-rate timelapse imagery that captures the onset of calving events. Event onsets are investigated in detail

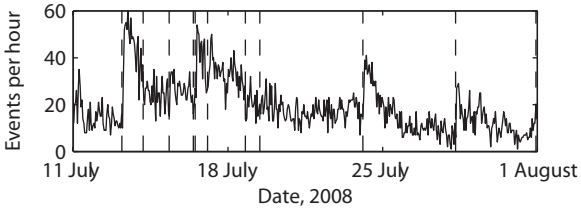

Figure 3.7. Temporal variations in the rates of short seismic events (Type I and II combined). Calving events are indicated by dashed vertical lines.

to determine whether calving events are triggered by motion of the mélange away from the terminus.

The first sign of an impending calving event in the 10-s timelapse imagery is generally either wide-spread fracturing (see spray of ice particles caused by seracs collapsing upglacier from the terminus in Videos 3.A-2 and 3.A-3) or avalanching of debris from the terminus (Video 3.A-4). No previous motion could be detected by either feature tracking in oblique imagery or by differencing subsequent images. A small, gradual increase in seismic activity often precedes discernible motion of the terminus and ice mélange in the 10-s imagery (Figs. 3.3c and 3.6a–b and Video 3.A-3, which shows the calving event discussed in Fig. 3.6). The ramp-up in seismic activity coincides with an increase in the number of audible fractures and, to a lesser extent, debris avalanches, emanating from the fjord (see Section 3.3.3; Fig. 3.6d). These sounds originate both at the terminus and in the fjord and are separated by periods of silence (i.e., there is no persistent background rumbling that is heard during calving events). We have so far been unable to detect any spatio-temporal patterns of acoustic signals preceding a calving event.

The increases in seismic energy and number of acoustic signals in the short interval preceding discernible motion at the terminus also precede observed horizontal acceleration of the ice mélange (Fig. 3.3c). Thus, motion of the mélange away from the terminus is not prerequisite for calving. The precursory activity in the fjord may instead represent unsettling of the mélange in response to a very small rotation of a large ice block at the glacier terminus. For example, rotating a 400 m long (in the glacier flow direction) by 1000 m tall iceberg by 0.5° will displace more than 4000 m^3 of water per meter of lateral width

of the iceberg, yet the upper corner of the iceberg (point P_1 in Fig. 3.8a) will move less than 0.02 m horizontally and 2 m vertically, while the point where the iceberg is in contact with the mélange (point P_2) will move 1 m horizontally. Such a small rotation at the terminus would therefore be undetectable with timelapse photography or our GPS receivers, but may be sufficiently large to cause near-terminus icebergs to subtly shift their positions and thereby generate seismic and acoustic signals. We suggest that the emergent onsets of the seismograms represent the superposition of numerous fractures occurring at the terminus and in the mélange.

Much of the seismic energy released during calving events at Jakobshavn Isbræ can, for several reasons, be attributed to horizontal and vertical motion of the ice mélange. First, maximum ground displacement coincides with the generation of large ocean waves, occuring immediately following the overturning of icebergs at the terminus (Video 3.A-3, Fig. 3.6a). Second, ground displacement during the coda of the seismograms, which typically lasts 10 min or more, represents motion of the mélange only (i.e., the terminus is quiescent). The coda of the seismogram therefore puts a minimum bound on the amount of ground displacement that can be generated through horizontal motion of the mélange. Third, there is a pronounced drop in seismic energy coincident with mélange stiffening as icebergs within the mélange have stopped overturning and the mélange has resumed steady deformation. Finally, the envelopes of the calving-generated seismic and acoustic waves have similar durations and several peaks that are temporally correlated, suggesting that the seismic and acoustic waves have the same source. As discussed earlier, many of the acoustic signals emanate from the ice mélange.

Calving-related seismograms are likely generated by a variety of mechanisms occurring simultaneously at numerous locations; they are therefore highly complex. Source mechanisms might include hydraulically-driven fracture propagation and other hydraulic transients within the glacier [*St. Lawrence and Qamar*, 1979; *Métaxian et al.*, 2003; *O'Neel and Pfeffer*, 2007; *Winberry et al.*, 2009], the coalescence of micro-fractures at the terminus [*Bahr*, 1995], acceleration of the glacier terminus [*Nettles et al.*, 2008], ocean wave action

[*Amundson et al.*, 2008; *MacAyeal et al.*, 2009], icebergs scraping the glacier terminus and fjord walls [*Amundson et al.*, 2008; *Tsai et al.*, 2008], and motion of an ice mélange or layer of sea ice. Superposition of these seismic signals makes interpretation of calving-generated seismograms exceedingly difficult. The interpretations can be improved with, among other things, simultaneous acoustic (including infrasonic and hydroacoustic) recordings. Glaciogenic acoustic signals are more impulsive and decay more rapidly than corresponding seismic signals (Fig. 3.6b,d). Identifying and locating events may therefore be somewhat easier with acoustic recordings than with seismic recordings (see also J. Richardson, manuscript in preparation, 2009).

3.5 Simple Force Balance Analysis of Calving

Motion of the ice mélange is clearly driven by terminus dynamics. The relationship is not, however, unidirectional. Here, we use a simple force balance analysis to argue that the mélange influences the seasonality of calving events and the sequence of individual calving events, including iceberg size and rotation direction. The force balance analysis also demonstrates that full-glacier-thickness icebergs, which dominate the glacier's mass loss from calving, are unable to calve from a well-grounded terminus.

First, consider the case in which a rectangular iceberg of thickness H and width εH (perpendicular to the terminus) calves from a floating tongue (Fig. 3.8a–b). Rotation of the iceberg is driven by buoyant forces and, ignoring friction, inhibited by contact forces at the terminus, F_t, and the mélange, F_m. For simplicity, we assume that the force from the mélange can be treated as a horizontal line load acting at sea level, so that $|F_t| = |F_m|$.

Summing the torques around the iceberg's center of mass for a block that is rotating bottom out (Fig. 3.8a), we find that F_m required to hold the block in static equilibrium for some given tilt angle, θ, is

$$F_m^b = \frac{-\sum_{i=1}^{3} \tau_i}{\gamma \cos\theta}, \tag{3.1}$$

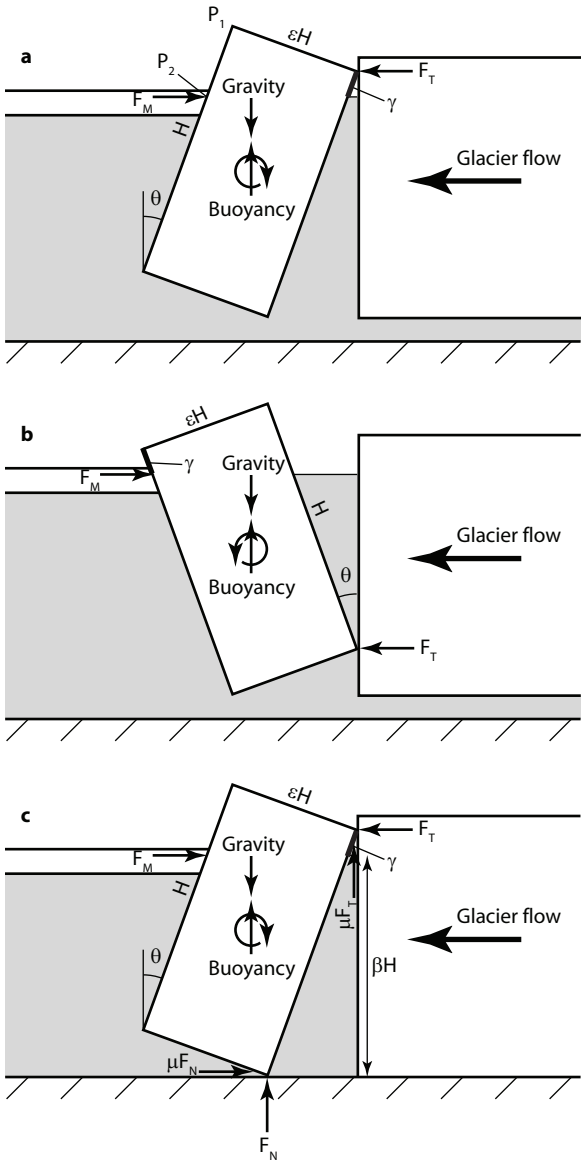

Figure 3.8. Diagrams used for the force balance analysis of calving icebergs. γ is indicated by thick black lines.

where superscript b denotes bottom out rotation, τ_i represents the torques from the water pressure acting along each of the iceberg's three submerged sides, $\gamma = H(1 - \rho_i/\rho_w - (\varepsilon/2)\tan\theta)$ (see Fig. 3.8 for the geometric interpretation of γ), and ρ_i and ρ_w are the densities of ice and water, respectively [adapted from *MacAyeal et al.*, 2003]. If the force from the mélange is

greater than the value given in Equation 3.1, then the torques on the iceberg will either decelerate an iceberg's rotation or prevent an iceberg from rotating in the first place.

Similarly, the force from the melange required to keep the block from rotating top out (Fig. 3.8b) is

$$F_m^t = \frac{-\sum_{i=1}^{3} \tau_i}{H(\cos\theta - \varepsilon\sin\theta) - \gamma\cos\theta} \tag{3.2}$$

where superscript t denotes top out rotation. The ratio of these two forces is

$$\frac{F_m^b}{F_m^t} = \frac{\cos\theta - \varepsilon\sin\theta}{(1 - \rho_i/\rho_w - (\varepsilon/2)\tan\theta)\cos\theta} - 1. \tag{3.3}$$

In the limit that $\theta \to 0$, this ratio becomes

$$\frac{F_m^b}{F_m^t} = \frac{\rho_i}{\rho_w - \rho_i} \approx 9. \tag{3.4}$$

At small θ the force from the mélange required to keep a block from rotating bottom out is roughly one order of magnitude greater than the force required to keep a block from rotating top out. In other words, the resistive torque from a given F_m is greater for an ice block that is rotating top out than it is for a block that is rotating bottom out. Thus, in the presence of a resistive ice mélange, bottom out rotation is strongly preferred over top out rotation. Without a mélange, there is no preferred direction of rotation in this simple, frictionless model.

The force from the mélange (Eq. 3.1) required to maintain static equilibrium is ultimately a function of H, ε, and θ. By arbitrarily setting H = 1000 m, approximately equal to the terminus thickness of Jakobshavn Isbræ, and using the equations for τ_i derived in *MacAyeal et al.* [2003], we can investigate the relationship between F_m^b and ε for various θ (Fig. 3.9a).

The maximum value of ε for which buoyant forces will cause an iceberg to overturn at arbitrarily small θ is $\varepsilon_{cr} \approx 0.73$. Furthermore, the largest force required from the ice mélange to prevent rotation occurs when $\varepsilon = \varepsilon_o \approx 0.42$; icebergs of this geometry are therefore more

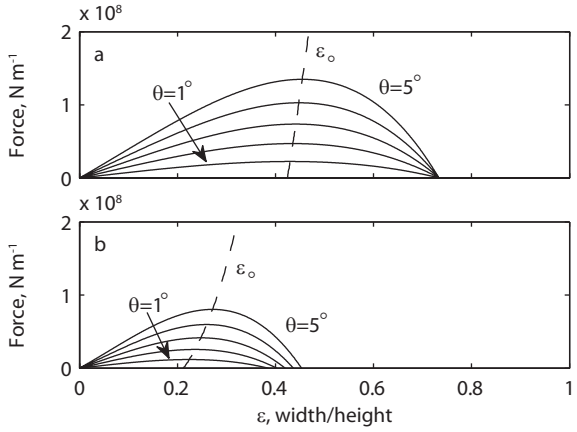

Figure 3.9. Force from the ice mélange (per meter lateral width) for various ε and θ that is required to decelerate an already overturning iceberg or to prevent an iceberg from overturning in the first place. These calculations assume that there is no friction at the contact points. Calving is considered from (a) a floating terminus and (b) a terminus that is at floatation ($\beta = \rho_i/\rho_w$). The dashed lines give the value of ε_o for various θ.

easily able to capsize than thinner or wider icebergs. In this model, ε_o corresponds to the iceberg geometry that experiences the largest buoyancy-driven torque at small θ.

If the terminus is instead grounded (Fig. 3.8c, with $\mu = 0$), the force and torque balances give

$$F_m^b = \frac{-\sum_{i=1}^{3} \tau_i - H/2\,(F_g - F_b)\,(\varepsilon\cos\theta - \sin\theta)}{H(\cos\theta - \beta)}. \tag{3.5}$$

where F_g and F_b are the gravitational and buoyant forces, $\beta = H_w/H$ and H_w is the water depth at the terminus, τ_i is the same as before, but γ (on which τ_i depends) is replaced with

$$\gamma = H(1 - \beta\sec\theta). \tag{3.6}$$

Here, when the terminus is just grounded (i.e., $\beta = \rho_i/\rho_w \approx 0.9$), $\varepsilon_{cr} = 0.40$ and $\varepsilon_o = 0.21$ for small θ (Fig. 3.9). At certain water depths, a terminus may be floating but at such an elevation that calving icebergs will come into contact with the fjord bottom during overturning. In such cases, ε_{cr} and ε_o will be intermediate to the values given above.

Including friction and/or lowering the water level below floatation further reduces ε_{cr}, ε_o, and the resistive force from the mélange required to prevent overturning. For example, ignoring the mélange (letting $F_m = 0$) but accounting for friction at the terminus and fjord bottom, the force and torque balances on the calving iceberg (Fig. 3.8c) become

$$F_t - \mu F_n = 0 \tag{3.7}$$

$$\mu F_t + F_n = F_g - F_b \tag{3.8}$$

$$\tau = \sum_{i=1}^{3} \tau_i + F_t H \left(\cos\theta + \frac{\mu}{2} (\sin\theta + \varepsilon \cos\theta) \right) + F_n \frac{H}{2} (\varepsilon \cos\theta - \sin\theta), \tag{3.9}$$

where F_n is the normal force on the fjord bottom, τ is the net torque acting on the iceberg, and μ is the coefficient of friction between the iceberg and the terminus and the iceberg and the fjord bottom (for simplicity, we assume that the coefficients of friction are the same for both points of contact). The curves in Figure 3.10 indicate the points at which $\tau = 0$ for various μ, ε, θ, and β. μ was varied from 0–0.1; these values are less than the coefficient of friction between ice and sand determined by sliding a relatively smooth, meter-scale ice block across a sand beach [*Barker and Timco*, 2003]. In order for buoyant forces to cause an iceberg of a given width-to-height ratio to overturn, the point in $\beta - \theta$ space must be above the appropriate $\tau = 0$ curve. From these curves it is apparent that buoyant forces are unable to cause the calving of realistically-sized, full-glacier-thickness icebergs unless the water depth is close to or greater than $\frac{\rho_i}{\rho_w} H$ (Fig. 3.10). A resistive ice mélange, not accounted for here, would further reduce the glacier's ability to calve from a grounded terminus, even if full-thickness fracture has occurred.

3.6 Interpretation

3.6.1 Mélange and Fjord Dynamics

Motion of the ice mélange is driven by terminus dynamics. Between calving events the mélange is pushed down fjord by the advancing terminus [see also *Joughin et al.*, 2008c]. During these periods ocean and wind currents have little effect on mélange motion, at least within 15–20 km of the glacier terminus (Video 3.A-1). Previously, however, ephemeral

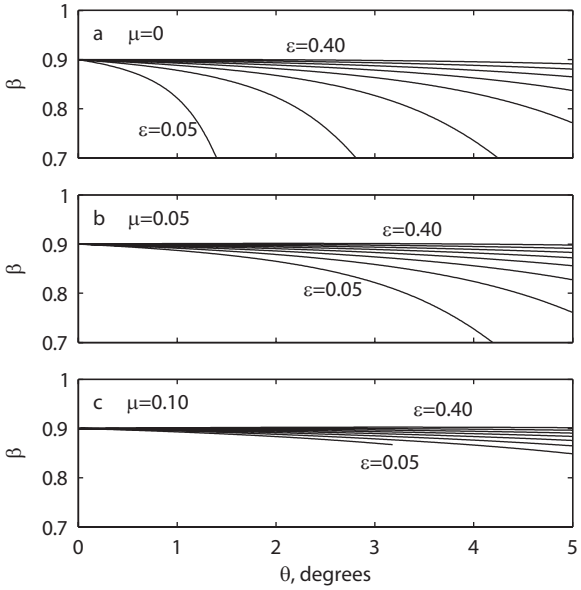

Figure 3.10. Minimum β (water depth divided by ice thickness) for which buoyant forces will cause a grounded iceberg with width εH and tilt from vertical θ to overturn. Coefficients of friction, μ, between the iceberg and terminus and iceberg and fjord bottom were varied from 0–0.1 ((a)–(c)).

turbid upwellings were observed at the terminus [*Echelmeyer and Harrison*, 1990], indicating that subglacial discharge occasionally caused local separation between the mélange and terminus. We observed no such upwellings during 2007–2008, thus suggesting that the recent increase in the glacier's calving flux has resulted in a denser, stronger mélange. Such changes may affect glacier dynamics (Section 3.6.2), the timing and sequence of calving events (Section 3.6.3), and damping of ocean waves [e.g., *Squire*, 2007, and references therein].

As full-glacier-thickness icebergs calve and overturn, they rapidly push the ice mélange down fjord (Fig. 3.3), sweep through $\sim$0.5 km^3 of water as they rotate through 90°, and may disrupt fjord stratification and circulation [as described in *Motyka et al.*, 2003] by turbulently mixing the entire water column. The total volume of water affected by a single calving iceberg is likely larger than 0.5 km^3, since water must fill the void left by the calving iceberg at the same time that water is being pushed down fjord by the rotating iceberg. A

typical calving event involves the calving of several full-glacier-thickness icebergs, which combined might displace more than 2 km^3 of water. Roughly thirty such calving events occur each year [*Amundson et al.*, 2008]. For comparison, the glacier's subglacial discharge, which drives fjord circulation, was estimated at 8–15 $km^3 a^{-1}$ in the 1980's [*Echelmeyer et al.*, 1992]. Thus calving events may strongly influence fjord circulation and affect the ability of deep, warm ocean water to reach the terminus. In a mélange-covered fjord, ocean currents may be further influenced by the irregular basal topography of the mélange.

The currents and meters-scale ocean waves generated by calving events may help icebergs rotate to more energetically favorable positions (with larger width to height ratios), resulting in extension of the mélange [see also *MacAyeal et al.*, 2009]. Although the mélange is eventually recompacted by the advancing terminus (following calving events the mélange is initally moving slower than the terminus; Fig. 3.3a,b), extension of the mélange during calving events may weaken it and reduce its ability to prevent subsequent calving events. Such weakening may explain, in part, why calving events occur more frequently in mid- to late summer and nearly always involve the successive calving of several icebergs [*Amundson et al.*, 2008].

3.6.2 Mélange Influence on Glacier Dynamics

The force required to prevent the calving and overturning of an iceberg at the glacier terminus (Fig. 3.9) is comparable to the change in back-force on the terminus due to tides. If the tidal range is 2 m and the mean water depth is 800 m, the range in back-force, ΔF_p is

$$\Delta F_p = \frac{1}{2}\rho_w g \left(801^2 - 799^2\right) \approx 1.6 \times 10^7 \mathrm{N\ m^{-1}}. \tag{3.10}$$

Tides appear to have little to no effect on the glacier's flow speed [see also Fig. 1b in *Amundson et al.*, 2008], especially when compared to other tidewater glaciers such as Columbia Glacier, Alaska [*Walters and Dunlap*, 1987]. Thus the mélange does not necessarily have a significant, direct influence on glacier velocity.

On the other hand, our results show that the mélange can inhibit calving, thereby helping to enable terminus advance in winter. The floating tongue that currently develops in

winter may be little more than an agglomeration of ice blocks that are unable to overturn (such as the partially overturned iceberg in Fig. 3.2b). Nonetheless, the newly-formed floating tongue reduces the longitudinal strain rates at the grounding line, resulting in thickening and an associated increase in effective (ice-overburden minus pore-water) pressure there. Basal motion is generally thought to be highly sensitive to effective pressure, especially when the effective pressure is close to zero [e.g., *Paterson*, 1994, and references therein], as is likely the case near the termini of tidewater glaciers [*Pfeffer*, 2007]. Thus a slight thickening near the grounding line in winter may be sufficient to explain the glacier's current seasonal velocity variations. Furthermore, the winter advance changes the geometry and stress distribution of the lower glacier; such changes have been shown to dramatically affect the glacier's flow, even without the inclusion of potential buttressing effects along the fjord walls (M.P. Lüthi, manuscript in preparation, 2009).

3.6.3 Sequence of Calving Events and Glacial Earthquakes

Although the mélange may not directly influence glacier motion, it may affect the sequence of individual calving events. In Section 3.5 we demonstrated that in the presence of a back force from the mélange, bottom out rotation of calving icebergs is strongly preferred over top out rotation and that icebergs with optimal width-to-height ratios ($\varepsilon = \varepsilon_o$) are more easily able to calve than icebergs of different dimensions. ε_o depends on the glacier's proximity to floatation and the coefficients of friction at points of contact with the terminus and fjord bottom, but is always less than 0.42 (Fig. 3.9). Our observations indicate that ε for full-glacier-thickness icebergs that calve and overturn is generally between 0.2 and 0.5 (Videos 3.A-2–3.A-4).

The force balance analysis, which is consistent with our field observations, suggests that calving events begin with the bottom out rotation of icebergs with relatively small width-to-height ratios. Calving onset may be aided by avalanching of the terminus, which increases the buoyant torque on the newly-formed iceberg, and/or by a subglacial outburst flood that rotates the iceberg away from the terminus [see also *O'Neel et al.*, 2007].

As the first iceberg calves, the mélange is pushed away from the terminus, both by the rotating iceberg and potentially by turbulent ocean currents generated by the rotating iceberg. Due to a reduction in back forces as the mélange accelerates away from the terminus, subsequent calving icebergs can more easily calve from a grounded terminus, rotate top out, and have larger width-to-height ratios. The latter two points are consistent with observations from the time-lapse imagery (see Videos 3.A-2 and 3.A-4). Furthermore, glacial earthquakes have recently been associated with calving events [*Joughin et al.*, 2008a; *Tsai et al.*, 2008; *Amundson et al.*, 2008; *Nettles et al.*, 2008] and hypothesized to be generated by especially large icebergs pushing off of the terminus [*Tsai et al.*, 2008] or scraping the fjord bottom [*Amundson et al.*, 2008]. If either of these glacial earthquake mechanisms is correct, then glacial earthquake generation should occur several minutes after calving onset, as has been observed (see *Amundson et al.* [2008], Fig. 3.A-4; *Nettles et al.* [2008], Fig. 3).

The value of ε_o may affect the timing of calving events. For example, if a crevasse penetrates the entire glacier thickness at some distance $\varepsilon_o H$ from the glacier terminus, the resulting iceberg may calve more readily than if the crevasse had penetrated the entire glacier thickness at a distance of $\varepsilon H \neq \varepsilon_o H$ from the terminus.

Our analysis has mostly neglected the relationship between the mélange and the calving of tabular ($\varepsilon \geq 1$) or nearly tabular ($\varepsilon_{cr} \leq \varepsilon \leq 1$) icebergs, which presently occurs during spring and winter when all or part of the terminus is floating and previously occurred year round. Although our observations on the generation of tabular and near-tabular icebergs are limited, we have twice witnessed the calving of tabular icebergs at the end of long calving events (Video 3.A-5) during the month of May. Both of these icebergs originated near the centerline of the glacier, where the terminus appeared to be partially ungrounded. Tabular icebergs might therefore only be able to detach from the glacier's terminus after previous, overturning icebergs have calved and pushed the mélange away from the glacier.

Although the mélange may influence the timing and sequence of calving events, once a calving event begins and the mélange accelerates away from the terminus, the total mass loss during the event may be controlled by other factors and processes, such as pre-existing

fractures in the glacier [*Bahr*, 1995; *Benn et al.*, 2007, and references therein], the glacier's height above buoyancy [*Van der Veen*, 1996; *Vieli et al.*, 2001](see Section 3.6.4), and weakening of the terminus by large glaciogenic ocean waves [*MacAyeal et al.*, 2006, 2009]. The first point, that the total mass loss from a calving event is determined by the presence (or absence) of large rifts, is consistent with our visual observations. Thus, unless the back-force exerted by the mélange is strong enough to influence rifting, in summer the total mass loss from calving over time scales of weeks to months is likely controlled by glacier dynamics and not by mélange strength. On annual or longer time scales, the total mass loss from calving may be influenced by the proportion of the year during which the mélange is strong enough to prevent calving events [*Joughin et al.*, 2008c]. Thus the mélange can affect the seasonality of the terminus position, which in turn affects the glacier's longer term behavior.

3.6.4 Floatation Condition for Calving

The calving of full-glacier-thickness icebergs is likely necessary to balance Jakobshavn Isbræ's high flow rates: between large calving events the terminus can easily advance more than 100 m despite the frequent calving of small (meter to several meter scale) icebergs. However, full-glacier-thickness icebergs are unable to capsize at small θ if the terminus is well-grounded (Fig. 3.10; Section 3.5), even if full thickness fracture has occurred. Therefore a necessary, but not sufficient, condition for calving retreat is that the terminus is close to floatation. The ratio of water depth to ice thickness, β, necessary for calving depends on iceberg geometry and on the coefficients of friction at the iceberg's contact points; it is therefore difficult to assign a specific floatation condition for calving. However, for realistic iceberg geometries ($\varepsilon = 0.25$) and a likely conservative coefficient of friction ($\mu = 0.05$), buoyancy-driven capsize will not occur unless $\beta > 0.875$ (Fig. 3.10b).

Due to buoyancy differences between ice and water, the immediate result of a full-thickness calving event from a grounded terminus is to increase the terminus' height above floatation (unless the glacier has a reverse bedrock slope that is more than nine times the

surface slope). Thus, although full-thickness calving events can be enabled by processes that change the torque balance on the terminus, such as avalanching of debris or subglacial discharge events, such processes cannot drive terminus retreat over long time periods.

During its current retreat, Jakobshavn Isbræ's average rate of retreat was largest in the early 2000's [*Podlech and Weidick*, 2004; *Csatho et al.*, 2008] when the terminus was floating year round. By 2004 the glacier had stopped producing tabular icebergs in summer (as can be seen in satellite imagery), suggesting that the glacier had evolved to calve grounded (or nearly grounded) ice in summer. At that time there was also a sharp decrease in the glacier's average rate of retreat [*Joughin et al.*, 2008c]. One potential explanation for this change is that the process limiting the glacier's rate of retreat switched from rift propagation in floating ice to dynamic thinning of grounded ice, processes occurring over different time scales. Thus, as long as the terminus region is sufficiently fractured, a height-above-floatation calving criterion [as proposed by *Van der Veen*, 1996] may give a reasonable assessment of the glacier's late summer terminus position. Such a criterion, which does not account for fracturing, is unable to predict individual calving events or to explain the growth and decay of a short floating tongue in winter [*Benn et al.*, 2007].

3.7 Conclusions

Temporal variations in ice mélange strength can influence the evolution of Jakobshavn Isbræ's terminus position, and therefore glacier flow [see also M.P. Lüthi, manuscript in preparation, 2009; *Nick et al.*, 2009], by controlling the timing of calving events. Furthermore, motion of the ice mélange is strongly controlled by terminus dynamics, especially with respect to frequency and size of calving events.

In winter, sea ice growth between icebergs (freezing of the mélange matrix) and at the mélange's seaward edge acts to stengthen the mélange, thus preventing calving and enabling the terminus to advance $\sim$5 km. The mélange is pushed down fjord as a cohesive unit by the advancing terminus. The sea ice margin begins to retreat from the fjord mouth in mid-winter; calving rejuvenates in spring after the sea ice margin has retreated to within

a few kilometers of the glacier terminus. Once calving renews, motion of the mélange becomes highly episodic, especially during periods of frequent calving. Large, full-glacier-thickness calving events cause the mélange to rapidly move 2–4 km down fjord, extend longitudinally, and be subjected to vertical oscillations lasting over 12 hrs and having peak amplitudes greater than 1 m. This wave action may promote further disintegration of the terminus and ice mélange [as also suggested by *MacAyeal et al.*, 2006, 2009], resulting in additional seaward expansion and thinning of the mélange. Between calving events the mélange is re-compressed and pushed forward by the advancing terminus, as occurs throughout winter.

Our observations and simple force balance analysis demonstrate that the presence of a mélange influences calving behavior: the first iceberg to calve tends to be small and always rotates bottom out, whereas subsequent calving icebergs can be larger and rotate any direction. Motion of the mélange away from the terminus does not appear to be prerequisite for calving to begin. However, when the mélange is activated during calving onset, it loses the ability to resist the calving of subsequent icebergs. The total amount of ice lost during a calving event is therefore likely controlled by parameters other than mélange strength, such as the presence (or absence) of pre-existing rifts up-glacier. Thus it is unlikely that the ice mélange controls the net calving flux in summer over time periods of days to weeks. Over seasonal time scales or longer, the mélange could influence the net calving flux by controlling the proportion of the year during which calving can occur [*Joughin et al.*, 2008c]. Although the resistive force from the mélange may be insufficient to directly influence glacier motion, the mélange may indirectly influence glacier dynamics by controlling the evolution of the terminus geometry, which in turn affects glacier motion (M.P. Lüthi, manuscript in preparation, 2009). Finally, the calving behavior observed at Jakobshavn Isbræ is unable to occur when the glacier is well-grounded (especially in the presence of a resistive ice mélange), suggesting that the net annual calving retreat is limited by the glacier's height above floatation.

A realistic model of terminus behavior must be able to predict seasonal variations in

calving rate. We suggest that at Jakobshavn Isbræ, these variations are presently controlled by variations in sea ice cover and ice mélange strength and by dynamic thinning of grounded ice in summer. The greater challenge is to couple the seasonality of ice mélange strength to the growth and decay of sea ice.

Acknowledgments

We thank D. Maxwell and G. Aðalgeirsdóttir for assistance with field work, and D.R. Fatland for loaning GPS receivers. Logistics and instrumental support were provided by CH2M Hill Polar Services and PASSCAL. Work in this manuscript was influenced by discussions with V.C. Tsai and D.R. MacAyeal. Comments from S. O'Neel, D. Benn, and an anonymous reviewer improved the clarity of the manuscript. Funding was provided by NASA's Cryospheric Sciences Program (NNG06GB49G), the U.S. National Science Foundation (ARC0531075), the Swiss National Science Foundation (200021-113503/1), the Comer Science and Education Foundation, an International Polar Year student traineeship funded by the Cooperative Institute for Arctic Research (CIFAR) through cooperative agreement NA17RJ1224 with the National Oceanic and Atmospheric Administration, and a UAF Center for Global Change Student Award also funded by CIFAR.

References

Abdalati, W., W. Krabill, E. Frederick, S. Manizade, C. Martin, J. Sonntag, R. Swift, R. Thomas, W. Wright, and J. Yungel (2001), Outlet glacier and margin elevation changes: Near-coastal thinning of the Greenland Ice Sheet, *J. Geophys. Res.*, *106*(D24), 33729–33741.

Amundson, J.M., M. Truffer, M.P. Lüthi, M. Fahnestock, M. West, and R.J. Motyka (2008), Glacier, fjord, and seismic response to recent large calving events, Jakobshavn Isbræ, Greenland, *Geophys. Res. Lett.*, *35*(L22501), doi:10.1029/2008GL035281.

Bahr, D.B. (1995), Simulating iceberg calving with a percolation model, *J. Geophys. Res.*, *100*(B4), 6225–6232.

Barker, A. and G. Timco (2003), The friction coefficient for a large ice block on a sand/gravel beach. *In* 12th Workshop on the Hydraulics of Ice Cover Rivers. CGU HS Committee on River Ice Processes and the Environment: Edmonton, AB, Canada.

Benn, D.I., C.R. Warren, and R.H. Mottram (2007), Calving processes and the dynamics of calving glaciers, *Earth Sci. Rev.*, *82*, 143–179.

Birnie, R.V. and J.M. Williams (1985), Monitoring iceberg production using LANDSAT, *Proceedings of the University of Dundee Summer School*, European Space Agency SP-216, 165–167.

Braun, M., A. Humbert, and A. Moll (2009), Changes of Wilkins Ice Shelf over the past 15 years and inferences on its stability, *Cryosphere*, *3*, 41–56.

Copland, L., D.R. Mueller, and L. Weir (2007), Rapid loss of the Ayles Ice Shelf, Ellesmere Island, Canada, *Geophys. Res. Lett.*, *34*(L21501), doi:10.1029/2007GL031809.

Csatho, B., T. Schenk, C.J. Van der Veen, and W.B. Krabill (2008), Intermittent thinning of Jakobshavn Isbræ, West Greenland, since the Little Ice Age, *J. Glaciol.*, *54*(184), 131–144.

Dean, R.G. and R.A. Dalrymple (1991), *Water Wave Mechanics for Engineers and Scientists*, 353 pp., World Scientific, Singapore.

Echelmeyer, K. and W.D. Harrison (1990), Jakobshavns Isbræ, West Greenland: Seasonal variations in velocity — or lack thereof, *J. Glaciol.*, *36*(122), 82–88.

Echelmeyer, K., W.D. Harrison, T.S. Clarke, and C. Benson (1992), Surficial glaciology of Jakobshavns Isbræ, West Greenland: Part II. Ablation, accumulation and temperature, *J. Glaciol.*, *38*(128), 169–181.

Geirsdóttir, Á., G.H. Miller, N.J. Wattrus, H. Björnsson, and K. Thors (2008), Stabilization of glaciers terminating in closed water bodies: Evidence and broader implications, *Geophys. Res. Lett.*, *35*(L17502), doi:10.1029/2008GL034432.

Higgins, A.K. (1991), North Greenland glacier velocities and calf ice production, *Polarforschung*, *60*(1), 1–23.

Holland, D.M., R.H. Thomas, B. DeYoung, M.H. Ribergaard, and B. Lyberth (2008), Acceleration of Jakobshavn Isbræ triggered by warm subsurface ocean waters, *Nature Geoscience*, *1*, 659–664, doi:10.1038/ngeo316.

Howat, I.M., I. Joughin, S. Tulaczyk, and S. Gogineni (2005), Rapid retreat and acceleration of Helheim Glacier, east Greenland, *Geophys. Res. Lett.*, *32*(L22502), doi:10.1029/2005GL024737.

Howat, I.M., I. Joughin, M. Fahnestock, B.E. Smith, and T.A. Scambos (2008), Synchronous retreat and acceleration of southeast Greenland outlet glaciers 2000–06: ice dynamics and coupling to climate, *J. Glaciol.*, *54*(187), 646–660.

Joughin, I., W. Abdalati, and M. Fahnestock (2004), Large fluctuations in speed on Greenland's Jakobshavn Isbræ glacier, *Nature*, *432*, 608–610.

Joughin, I., I. Howat, R. B. Alley, G. Ekstrom, M. Fahnestock, T. Moon, M. Nettles, M. Truffer, and V. C. Tsai (2008a), Ice-front variation and tidewater behavior on Helheim and Kangerdlugssuaq Glaciers, Greenland, *J. Geophys. Res.*, *113*(F01004), doi:10.1029/2007JF000837.

Joughin, I., S.B. Das, M.A. King, B.E. Smith, I.M. Howat, and T. Moon (2008b), Seasonal speedup along the western flank of the Greenland Ice Sheet, *Science*, *320*(5877), doi:10.1126/science.1153288.

Joughin, I., I.M. Howat, M. Fahnestock, B. Smith, W. Krabill, R.B. Alley, H. Stern, and M. Truffer (2008c), Continued evolution of Jakobshavn Isbræ following its rapid speedup, *J. Geophys. Res. - Earth Surface*, *113*(F04006), doi:10.1029/2008JF001023.

Krabill, W., E. Hanna, P. Huybrechts, W. Abdalati, J. Cappelen, B. Csatho, E. Frederick, S. Manizade, C. Martin, J. Sonntag, R. Swift, R. Thomas, and J. Yungel (2004), Greenland Ice Sheet: Increased coastal thinning, *Geophys. Res. Lett.*, *31*(L24402), doi:10.1029/2004GL021533.

Luckman, A., T. Murray, R. de Lange, and E. Hanna (2006). Rapid and synchronous ice-dynamic changes in East Greenland, *Geophys. Res. Lett.*, *33*(L03503), doi:03510.01029/2005GL025428.

Lüthi, M.P., M. Fahnestock, and M. Truffer (2009), Calving icebergs indicate a thick layer of temperate ice at the base of Jakobshavn Isbræ, Greenland, *J. Glaciol.*, *55*(191), 563–566.

MacAyeal, D.R., T.A. Scambos, C.L. Hulbe, and M.A. Fahnestock (2003), Catastrophic ice-shelf break-up by an ice-shelf-fragment-capsize mechanism, *J. Glaciol.*, *49*(164), 22–36.

MacAyeal, D.R., E.A. Okal, R.C. Aster, J.N. Bassis, K.M. Brunt, L. Mac. Cathles, R. Drucker, H.A. Fricker, Y.-J. Kim, S. Martin, M.H. Okal, O.V. Sergienko, M.P. Sponsler, and J.E. Thom (2006), Transoceanic wave propagation links iceberg calving margins of Antarctica with storms in tropics and Northern Hemisphere, *33*(L17502), doi:10.1029/2006GL027235.

MacAyeal, D.R., E.A. Okal, R.C. Aster, and J.N. Bassis (2009), Seismic observations of glaciogenic ocean waves (micro-tsunamis) on icebergs and ice shelves, *J. Glaciol.*, *55*(190), 193–206.

Métaxian, J.-P., S. Araujo, M. Mora, and P. Lesage (2003), Seismicity related to the glacier of Cotopaxi Volcano, Ecuador, *Geophys. Res. Lett.*, *30*(9), 1483, doi:10.1029/2002GL016773.

Moon, T. and I. Joughin (2008), Changes in ice front position on Greenland's outlet glaciers from 1992-2007, *J. Geophys. Res.*, *113*(F02022), doi:10.1029/2007JF000927.

Motyka, R.J., L. Hunter, K.A. Echelmeyer, and C. Connor (2003), Submarine melting at the terminus of a temperate tidewater glacier, LeConte Glacer, Alaska, U.S.A., *A. Glaciol.*,*36*, 57–65.

Nettles, M., T.B. Larsen, P. Elósegui, G.S. Hamilton, L.A. Stearns, A.P. Ahlstrøm, J.L. Davis, M.L. Andersen, J. de Juan, S.A. Khan, L. Stenseng, G. Ekström, and R. Forsberg (2008), Step-wise changes in glacier flow speed coincide with calving and glacial earthquakes at Helheim Glacier, Greenland, *Geophys. Res. Lett.*, *35*(L24503), doi:10.1029/2008GL036127.

Nick, F.M., A. Vieli, I.M. Howat, and I. Joughin (2009), Large-scale changes in Greenland outlet glacier dynamics triggered at the terminus, *Nature Geoscience*, doi:10.1038/NGEO394.

O'Neel, S., H.P. Marshall, D.E. McNamara, and W.T. Pfeffer (2007), Seismic detection and analysis of icequakes at Columbia Glacier, Alaska, *J. Geophys. Res.*, *112*(F03S23), doi:10.1029/2006JF000595.

O'Neel, S. and W.T. Pfeffer (2007), Source mechanics for monochromatic icequakes produced during iceberg calving at Columbia Glacier, AK, *Geophys. Res. Lett.*, *34*(L22502), doi:10.1029/2007GL031370.

Paterson, W.S.B. (1994), *The Physics of Glaciers, 3rd ed.*, 481 pp., Butterworth-Heinemann, Oxford.

Pfeffer, W.T. (2007), A simple mechanism for irreversible tidewater glacier retreat, *J. Geophys. Res.*, *112*(F03S25), doi:10.1029/2006JF000590.

Podlech, S. and A. Weidick (2004), A catastrophic break-up of the front of Jakobshavn Isbræ, West Greenland, 2002/2003, *J. Glaciol.*, *50*(168), 153–154.

Reeh, N. H.H. Thomsen, A.K. Higgins, and A. Weidick (2001), Sea ice and the stability of north and northeast Greenland floating glaciers, *A. Glaciol.*, *33*, 474–480.

Rignot, E. and P. Kanagaratnam (2006), Changes in the velocity structure of the Greenland Ice Sheet, *Science*, *311*(5763), 986–990, doi:10.1126/science.1121381.

St. Lawrence, W. and A. Qamar (1979), Hydraulic transients: A seismic source in volcanoes and glaciers, *Science*, *203*, 654–656.

Scambos, T., H.A. Fricker, C.-C. Liu, J. Bohlander, J. Fastook, A. Sargent, R. Massom, and A.-M. Wu (2009), Ice shelf disintegration by plate bending and hydro-fractures: Satellite observations and model results of the 2008 Wilkins ice shelf break-ups, *Earth Planet. Sci. Lett.*, *280*, 51–60.

Sohn, H.-G., K.C. Jezek, and C.J. van der Veen (1998), Jakobshavn Glacier, West Greenland: 30 years of spaceborne observations, *Geophys. Res. Lett.*, *25*(14), 2699–2702.

Squire, V.A. (2007), Of ocean waves and sea-ice revisited, *Cold Reg. Sci. Technol.*, *49*, 110–133.

Thomas, R.H. (1979), Ice Shelves: A Review, *J. Glaciol.*, *24*(90), 273–286.

Thomas, R.H., W. Abdalati, T.L. Akins, B.M. Csatho, E.B. Frederick, S.P. Gogineni, W.B. Krabill, S.S. Manizade, and E.J. Rignot (2000), Substantial thinning of a major east Greenland outlet glacier, *Geophys. Res. Lett.*, *27*(9), 1291–1294.

Tsai, V.C., J.R. Rice, and M. Fahnestock (2008), Possible mechanisms for glacial earthquakes, *J. Geophys. Res.–Earth Surfaces*, *113(F03014)*, doi:10.1029/2007JF000944.

Van der Veen, C.J. (1996), Tidewater calving, *J. Glaciol.*, *42*(141), 375–385.

Vieli, A., M. Funk, and H. Blatter (2001), Flow dynamics of tidewater glaciers: a numerical modelling approach, *J. Glaciol.*, *47*(59), 595–606.

Walters, R.A. and W.W. Dunlap (1987), Analysis of time series of glacier speed: Columbia Glacier, Alaska, *J. Geophys. Res.*, *92*(B9), 8969–8975.

Winberry, J.P., S. Anandakrishnan, and R.B. Alley (2009), Seismic observations of transient subglacial water-flow beneath MacAyeal Ice Stream, West Antarctica, *Geophys. Res. Lett.*, *36*(L11502), doi:10.1029/2009GL037730.

Appendix 3.A

The following supplementary videos are included in a DVD at the end of the thesis.

Video 3.A-1: Time-lapse video of Jakobshavn Isbrae's proglacial ice melange from 9 July-31 July 2008. The camera was positioned approximately 10 km down fjord from the terminus and pointed in the down fjord direction. The pulses in ice melange motion are due to calving events.

Video 3.A-2: Hi-rate (10 s) time-lapse video of a calving event on 10 May 2008. Iceberg detachment was preceded by widespread fracturing and the collapse of seracs some distance upglacier from the terminus.

Video 3.A-3: Hi-rate (10 s) time-lapse video of a calving event on 15 July 2008 (see also associated seismic and audio recordings in Figure 6). Iceberg detachment was preceded by widespread fracturing and the collapse of seracs some distance upglacier from the terminus.

Video 3.A-4: Hi-rate (10 s) time-lapse video of a calving event on 24 July 2008 (see also associated iceberg motion in Figure 3c). Large-scale calving was preceded by several debris avalanches from the terminus.

Video 3.A-5: Time-lapse video of a calving event on 16 May 2008 (the glacier terminus is just off the edge of the frame). Photos were taken every 10 min. A tabular iceberg was calved at the end of the calving event and appears at the end of the video.

Chapter 4
A unifying framework for iceberg calving models [1]

Abstract

We develop a general framework for iceberg calving models that can be applied to any calving margin. The framework is based on mass continuity, the assumption that calving rate and terminus velocity are not independent, and the simple idea that terminus thickness following a calving event is larger than terminus thickness at the event onset. The theoretical, near steady-state analysis used to formulate the framework indicates that calving rate is governed, to first order, by ice thickness, thickness gradient, dynamic thinning, and melting of the terminus; the analysis furthermore provides a physical explanation for the empirical relationship for ice shelf calving found by Alley and others [2008]. In the calving framework the pre- and post-calving terminus thicknesses are given by two unknown but related functions. The functions can vary independently of changes in glacier flow and geometry, and can therefore account for variations in calving behavior due to external forcings and/or self-sustaining calving processes. Although the calving framework does not constitute a complete calving model, any thickness-based calving criterion can easily be incorporated into the framework. The framework should be viewed as a guide for future attempts to parameterize calving.

4.1 Introduction

Iceberg calving is an important mechanism of mass loss for the Antarctic and Greenland Ice Sheets and many glaciers around the world [Jacobs and others, 1992; Hagen and others, 2003; Rignot and Kanagaratnam, 2006]. Observations of recent calving retreats and coincident flow acceleration at glaciers in Greenland and Antarctica [De Angelis and Skvarca, 2003; Joughin and others, 2004; Rignot and others, 2004; Howat and others, 2008] have

[1] Submitted to the *Journal of Glaciology* as Amundson, J.M. and M. Truffer. A unifying framework for iceberg calving models.

served to illustrate the tight linkages between calving, glacier flow, and terminus stability. Unfortunately, modeling of calving processes remains a major challenge, thus casting doubt on the ability of glacier and ice sheet models to predict future sea level variations.

A full calving model would describe the rapid (minutes to hours) evolution of glacier geometry and stress field that occurs as an ice block detaches from a glacier [e.g., Pralong and Funk, 2005]. Reconciling the high temporal and spatial resolution necessary for such a model with the computational constraints of ice sheet models is, however, a highly difficult task. An alternative is to seek a parameterization of calving that is sufficiently general to be applicable to any calving margin, yet sufficiently simple to be implementable in ice sheet models.

Previous efforts to parameterize calving include (1) relating mean calving rate of grounded glaciers to water depth at the terminus [Brown and others, 1982], (2) continuously adjusting the terminus position so that terminus thickness always equals some value given by a calving criterion [Van der Veen, 1996; Vieli and others, 2000, 2001; Benn and others, 2007a,b], and (3) relating mean calving rate of ice shelves to ice shelf thickness, width, and strain rate [Alley and others, 2008]. Unfortunately, none of the previous efforts fully addresses the wide range in size and frequency of calving events, and furthermore the model of Benn and others [2007a,b] is the only model that can clearly be applied to both floating and grounded termini. In their model, the terminus is located where crevasse depth equals terminus freeboard, with crevasse depth depending on longitudinal strain rates and ponding of water in crevasses.

Despite the advances made by Benn and others [2007a,b], their crevasse-depth calving criterion cannot explain all calving variability. As an example, consider the terminus dynamics of Jakobshavn Isbræ, a rapidly-flowing outlet glacier in Greenland. Currently, calving ceases during winter and the terminus advances ~ 5 km. Calving typically resumes vigorously in March or April, well before significant surface melting has occurred; within a few weeks the terminus can retreat 3–4 km. The terminus continues retreating, albeit at a slower rate, throughout the summer [Amundson and others, 2008]. The observed

seasonal variations in calving rate cannot be explained by the crevasse-depth calving criterion, as the onset of calving in spring precedes significant surface melting, ponding of melt water in near terminus crevasses is rare, seasonal variations in velocity (and therefore strain rates) are smaller than at other tidewater glaciers [Echelmeyer and Harrison, 1990], and velocity variations appear to occur in response to changes in terminus position and not vice-versa [Joughin and others, 2008b; Amundson and others, 2008]. The crevasse-depth calving criterion is furthermore inconsistent with the glacier's current terminus freeboard, which is about 100 m. The model would require strain rates of about 9 a^{-1}, or nearly an order of magnitude larger than observed [Amundson and others, 2008], to produce crevasses that are 100 m deep.

Parameterization of calving is confounded by the wide variety of calving phenomena, including the sub-hourly detachment of small ice blocks from grounded, temperate glaciers [O'Neel and others, 2003, 2007], the roughly decadal calving of giant tabular icebergs (with horizontal dimensions of 10–100 km) from floating ice shelves [Lazzara and others, 1999], and the catastrophic collapse of thin ice shelves within a matter of days to weeks [Rott and others, 1996; Scambos and others, 2000; Braun and others, 2009; Braun and Humbert, 2009]. Herein, we develop a broad framework for calving models that, unlike previous efforts, can be adapted to describe the wide range in size and frequency of calving events. The framework is based on the simple idea that terminus thickness is larger after a calving event than at the event onset, and that pre- and post-calving terminus thicknesses are given by two separate but related functions. The functions are left unspecified, and therefore new or existing calving models can be easily incorporated into the framework. We do, however, investigate the relationship between the functions by considering the wide spectrum of observed calving styles. In particular, the calving framework allows for a simple parameterization of the highly non-linear, chain-reaction type processes that can cause large portions of an ice shelf to disintegrate in a matter of days [see MacAyeal and others, 2009].

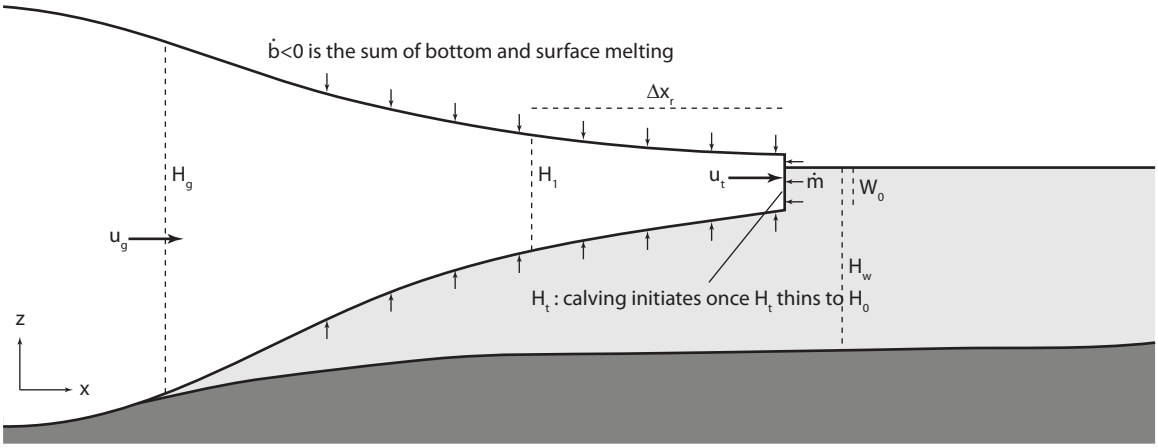

Figure 4.1. Schematic diagram of a glacier terminus indicating many of the variables used in the present analysis.

4.2 Steady-state calving rate

The following analysis is developed in two horizontal dimensions to ease possible implementation into glacier and ice sheet models. In two dimensions, the change in terminus position with time for a calving glacier is given by

$$\frac{d\mathbf{X}}{dt} = \mathbf{u_t} - \mathbf{u_c} - \dot{\mathbf{m}}, \tag{4.1}$$

where $\mathbf{X}$ is terminus position, t is time, $\mathbf{u_t}$, $\mathbf{u_c}$, and $\dot{\mathbf{m}}$ are the vertically-averaged along-flow terminus velocity, calving rate, and melt rate of the vertical face of the terminus [Motyka and others, 2003], respectively (Fig. 4.1), and bold face is used to indicate two-dimensional, horizontal vectors. We use $\dot{\mathbf{m}}$ to refer to both terminus melting and calving associated with non-uniform melting of the terminus (as discussed in Motyka and others [2003] and Röhl [2006]). Over annual time scales, terminus velocity and calving rate tend to scale with each other, such that the rate of length change is almost always one to two orders of magnitude smaller than terminus velocity (or calving rate)[Van der Veen, 1996]. The observation that calving rate and terminus velocity are two numbers of similar magnitude that almost exactly cancel indicates that they are not independent of each other.

Here, we use a steady-state analysis to show that ice thickness, thickness gradient, dynamic thinning, and melting of the terminus are the primary controls on calving rate

(and therefore also on terminus velocity). We furthermore show that a wide spectrum of calving behavior can be produced by simply increasing the terminus thickness during a calving event. For a given ratio of pre- to post-calving terminus thickness, thickness gradient determines the event size, and strain rate and balance rate determine the time it takes the terminus to thin back to a critical value at which calving occurs. The analysis presented here provides the basis for a general calving framework (Section 4.3).

4.2.1 Continuous calving

For a glacier that is in steady state, $d\mathbf{X}/dt = 0$. Calving rate is therefore given by

$$\mathbf{u_c} = \mathbf{u_t} - \dot{\mathbf{m}}. \tag{4.2}$$

Terminus velocity, $\mathbf{u_t}$, can be estimated through the mass continuity equation, which dictates that for a column of ice

$$\frac{\partial h}{\partial t} = \dot{b} - \nabla \cdot \mathbf{q}. \tag{4.3}$$

Here h is ice thickness, $\dot{b}$ is the combined surface and bottom melt rate, $\nabla = (\partial/\partial x, \partial/\partial y)$, and $\mathbf{q}$ is horizontal ice flux. We let $\overline{\mathbf{u}}$ equal the depth-averaged horizontal velocity, so that $\mathbf{q} = h\overline{\mathbf{u}}$ and Equation (4.3) becomes

$$\frac{\partial h}{\partial t} = \dot{b} - h\nabla \cdot \overline{\mathbf{u}} - \overline{\mathbf{u}} \cdot \nabla h, \tag{4.4}$$

We now note that

$$h\nabla \cdot \overline{\mathbf{u}} = h\frac{\partial}{\partial x}\left(\frac{1}{h}\int_0^h u \cdot dz\right) + h\frac{\partial}{\partial y}\left(\frac{1}{h}\int_0^h v \cdot dz\right), \tag{4.5}$$

where u and v are horizontal velocities within the column. Equation (4.5) is equivalent to

$$h\nabla \cdot \overline{\mathbf{u}} = -\overline{\mathbf{u}} \cdot \nabla h + h(\dot{\varepsilon}_{xx} + \dot{\varepsilon}_{yy}) + \mathbf{u_s} \cdot \nabla h, \tag{4.6}$$

where $\dot{\varepsilon}_{xx}$ and $\dot{\varepsilon}_{yy}$ are the depth-averaged normal strain rates and $\mathbf{u_s}$ is the horizontal surface velocity vector. Strain rates greater than 0 are used to indicate extension. As a result, $\nabla h < 0$ indicates that ice thickness decreases in the downglacier direction, as is generally observed near a glacier terminus.

Due to the incompressibility of ice,

$$\dot{\varepsilon}_{zz} = -\dot{\varepsilon}_{xx} - \dot{\varepsilon}_{yy}, \tag{4.7}$$

where $\dot{\varepsilon}_{zz}$ is the depth-averaged vertical normal strain rate.

Inserting Equation (4.7) into Equation (4.6), and the result into Equation (4.4), gives

$$\frac{\partial h}{\partial t} = \dot{b} + h\dot{\varepsilon}_{zz} - \mathbf{u_s} \cdot \nabla h. \tag{4.8}$$

For a glacier that is in steady-state, all terms in Equation (4.8) are temporally invariant and $\partial h/\partial t = 0$. Furthermore, near the terminus of a calving glacier, surface velocity, $\mathbf{u_s}$, and depth-averaged velocity are generally in close agreement regardless of whether the terminus is floating or grounded [e.g., Pfeffer, 2007]. Rearranging Equation (4.8), assuming that the glacier is in steady-state, and setting $\overline{\mathbf{u}} = \mathbf{u_s}$, gives

$$\overline{\mathbf{u}} \cdot \nabla h = \dot{b} + h\dot{\varepsilon}_{zz}, \tag{4.9}$$

which is satisfied when

$$\overline{\mathbf{u}} = \frac{(\dot{b} + h\dot{\varepsilon}_{zz})\nabla h}{|\nabla h|^2}. \tag{4.10}$$

Equation (4.10) is found by assuming that the velocity vector points in the direction of largest thickness gradient.

Finally, evaluating Equation (4.10) at or near the terminus and inserting the result into Equation (4.2) yields

$$\mathbf{u_c} = \frac{(\dot{b} + H_t\dot{\varepsilon}_{zz})\nabla h}{|\nabla h|^2} - \dot{\mathbf{m}}, \tag{4.11}$$

where H_t is terminus thickness. Equation (4.11) suggests that ice thickness, strain rate, and thickness gradient are the primary controls on calving rate. Balance rate and melting of the vertical face of the terminus also influence the steady-state calving rate but are typically less important.

4.2.2 Discrete calving

Under steady-state conditions, the position of a glacier terminus is fixed, and thus calving events must occur continuously and be infinitesimally small. We here consider how mean

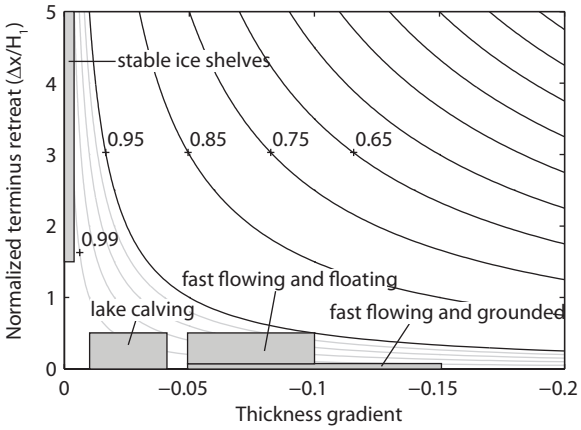

Figure 4.2. Contours of H_0/H_1 for various along-flow thickness gradients ($\partial h/\partial x$) and normalized calving retreat lengths ($\Delta x/H_1$). Gray contours represent intervals of 0.01. Shaded boxes indicate approximate thickness gradients and calving event sizes (see references in Benn and others [2007b]) for various calving margins during near steady-state conditions.

calving rate is affected by discrete calving events that occur periodically and are always the same size. Glacier strain rates, thickness gradient, and melt terms are held constant, but $d\mathbf{X}/dt \neq 0$. We furthermore assume that $\mathbf{u_c}$ and $\dot{\mathbf{m}}$ point in the direction of largest thickness gradient.

The distance, $\Delta\mathbf{x}$, that a point along the terminus retreats during a calving event is

$$\Delta\mathbf{x} = \frac{(H_0 - H_1)\nabla h}{|\nabla h|^2}, \tag{4.12}$$

where H_0 and H_1 are the terminus thicknesses at the onset of and immediately following calving events. The ratio of pre- to post-calving terminus thickness, H_0/H_1, is typically close to 1 (Fig. 4.2).

The thinning rate of a column of ice as it is advected toward the terminus is given by the material derivative

$$\frac{Dh}{Dt} = \frac{\partial h}{\partial t} + \overline{\mathbf{u}} \cdot \nabla h. \tag{4.13}$$

Inserting Equation (4.9) into Equation (4.13) and again assuming that $\overline{\mathbf{u}} = \mathbf{u_s}$ yields

$$\frac{Dh}{Dt} = h\dot{\varepsilon}_{zz} + \dot{b}. \tag{4.14}$$

The time interval between calving events, Δt, is determined by the time it takes the terminus to thin from H_1 to H_0. The column of ice that reaches the terminus at time Δt will have had an initial thickness of $H_1 - (\dot{\mathbf{m}} \cdot \nabla h)\Delta t$. Thus, integrating Equation (4.14) from $H_1 - (\dot{\mathbf{m}} \cdot \nabla h)\Delta t$ to H_0 gives

$$\Delta t = \frac{1}{\dot{\varepsilon}_{zz}} \ln \left(\frac{H_0 \dot{\varepsilon}_{zz} + \dot{b}}{H_1 \dot{\varepsilon}_{zz} + \dot{b} - (\dot{\mathbf{m}} \cdot \nabla h)\Delta t \dot{\varepsilon}_{zz}} \right). \tag{4.15}$$

The period between events depends inversely on vertical strain rate and becomes infinitesimally small as $H_1 \rightarrow H_0$. When strain rates are high, the ratio of pre- to post-calving terminus thickness, H_0/H_1, has little impact on the time period between events (Fig. 4.3). Similarly, melt-induced changes in terminus geometry most strongly impact the calving interval of slow flowing glaciers; high bottom and surface melting, $\dot{b}$, tends to decrease Δt (Fig. 4.3a), whereas high melting of the vertical face of the terminus, $\dot{\mathbf{m}}$, tends to increase Δt (Fig. 4.3b).

Over several calving events, the mean calving rate is

$$\mathbf{u_c} = \frac{\Delta \mathbf{x}}{\Delta t}. \tag{4.16}$$

Inserting Equation (4.12) into Equation (4.16) gives

$$\mathbf{u_c} = \frac{k H_0 \dot{\varepsilon}_{zz} \nabla h}{|\nabla h|^2}, \tag{4.17}$$

where k is a non-dimensional number given by

$$k = \frac{H_0 - H_1}{H_0 \dot{\varepsilon}_{zz} \Delta t}. \tag{4.18}$$

In general, $1 \leq k \leq 1.5$ (set $\dot{\mathbf{m}} \cdot \nabla h = 0$ in Equation (4.15), insert the result into Equation (4.18), and evaluate with appropriate values of all remaining variables). k is large for small H_0/H_1; thus, mean calving rate is slightly larger for glaciers that experience large calving events, even if the calving events do not affect the glacier flow field or thickness gradient, as has been assumed here. If calving events are large enough to cause upglacier acceleration and drawdown, then mean calving rate would be expected to further increase. Furthermore, in

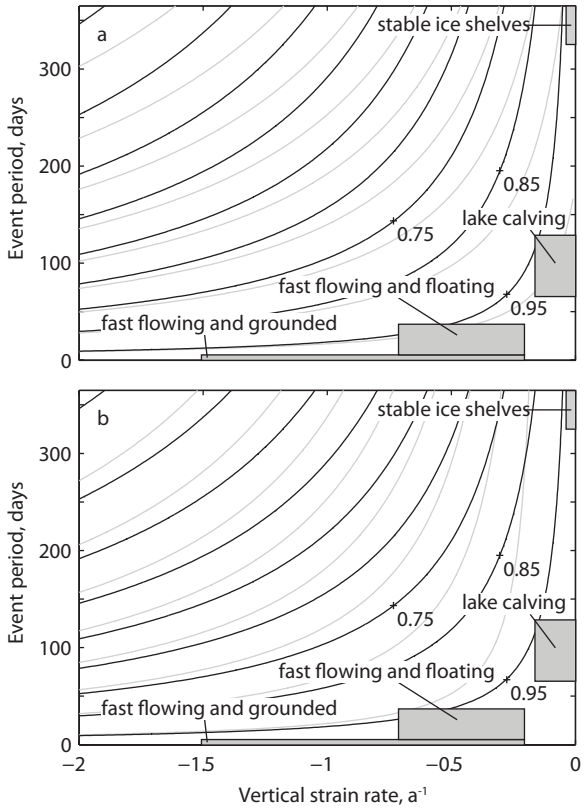

Figure 4.3. Contours of H_0/H_1 for various strain rates ($\dot{\varepsilon}_{zz}$), time periods between calving events (Δt), ice thicknesses (H_1), and along-flow melt rates ($\dot{b}$ and $\dot{m}$). In both panels, H_1 = 500 m and black curves indicate $\dot{b} = \dot{m} = 0$. Gray curves indicate that (a) $\dot{b} = -50$ m a^{-1} and $\dot{m} = 0$ (surface and bottom melting dominate over backwards melting of the terminus) and (b) $\dot{b} = 0$, $\dot{m} = 365$ m a^{-1}, and $\partial h/\partial x = -0.2$ (backwards melting of the terminus dominates over surface and bottom melting). Shaded boxes indicate approximate strain rates and calving intervals (see references in Benn and others [2007b]) for various calving margins during near steady-state conditions.

the limit that $H_1 \rightarrow H_0$, calving becomes continuous and Equation (4.17) reduces to Equation (4.11), as expected. Although Equations (4.11) and (4.17) are nearly equivalent, we prefer Equation (4.17) as the basis for a general calving framework because it accounts for the time dependent relationship between terminus thinning rate and terminus thickness (through Equation (4.14)) and can characterize a wide range of calving behavior (see Figs. 4.2 and 4.3).

4.2.3 Comparison with observations

The form of our near steady-state calving rate relation (Equation (4.17)) is consistent with the empirical relationship for ice-shelf calving found by Alley and others [2008]. By analyzing data from a variety of ice shelves, they found that calving rate (along a glacier flow line) could be estimated by

$$u_c = c \cdot (wH_t\dot{\varepsilon}_{xx}), \tag{4.19}$$

where u_c is set equal to terminus velocity u_t, w is terminus half-width, and c is an empirically-determined constant approximately equal to 0.016 m^{-1}. All parameters were measured within a few ice thicknesses of the terminus.

Using theoretical work and comparing the results to observations, Sanderson [1979] demonstrated that ice shelf half-width is related to along-flow thickness gradient, $\partial h/\partial x$, through the relationship

$$w = \frac{-2\tau}{\rho_i g(1-\rho_i/\rho_w)}\left(\frac{\partial h}{\partial x}\right)^{-1}, \tag{4.20}$$

where τ is the depth-averaged shear stress on the ice shelf margin, ρ_i and ρ_w are the densities of ice and water, g is gravitational acceleration, and x points in the downglacier direction. Inserting Equation (4.20) into Equation (4.19) and setting τ = 90 kPa [as also done by Sanderson, 1979] gives

$$u_c \approx -3H_t\dot{\varepsilon}_{xx}\left(\frac{\partial h}{\partial x}\right)^{-1}. \tag{4.21}$$

When melt terms and across-flow normal strain rates are negligible, the value of u_c in Equation (4.21) is roughly two to three times greater than our calving rate relation, but the form of the equations are otherwise identical.

The factor of two to three difference could be attributed to approximations in the theoretical work by Sanderson [1979](which should be trusted "only to within a factor of about two"), overestimation of shear stresses on the ice shelf margin (Crabtree and Doake [1982] used τ = 40 kPa), not accounting for melting of the terminus or lateral stretching, our assumption that near-terminus glacier flow is steady and spatially invariant, and measurement uncertainties or measurements in Alley and others [2008] being made farther

away from the terminus than is required by Equation (4.17). For example, the strain rates they cited for Jakobshavn Isbræ are roughly a factor of two smaller than was observed within a few kilometers of the terminus in the 1980's (Motyka et al., in review); if applied uniformly, a factor of two increase in near-terminus strain rate would result in a reduction of c by one-half. We thus argue that, using different approaches, we and Alley and others [2008] have demonstrated that the primary controls on mean calving rate are ice thickness, dynamic thinning, and thickness gradient (which is related to terminus width for ice shelves). Furthermore, our analysis applies for both grounded and floating termini, potentially explaining why the mean calving rate for Columbia Glacier, a grounded tidewater glacier, was consistent with the linear regression on floating ice shelves shown in Alley and others [2008]. Our calving rate relation, however, accounts for thinning of the terminus due to lateral stretching and melting; it therefore represents an improvement over the work of Alley and others [2008]. When applying our calving rate relation, strain rates, thickness gradient, and melt terms should be evaluated within a few ice thicknesses of the terminus.

4.3 Calving framework

4.3.1 General framework

In the previous section we argued that calving rate is controlled, to first order, by ice thickness, thickness gradient, dynamic thinning, and melting of the terminus. We also demonstrated that calving event size and periodicity can be characterized simply by changing the terminus thickness during a calving event (Equations (4.12) and (4.15)). Our analysis assumed steady-state or near steady-state conditions, and thus our calving rate relation (Equation (4.17)) is only valid for glaciers that are near steady-state. In reality all terms in Equation (4.17), including H_0 and H_1, vary in space and time. Furthermore, H_0 and H_1 are unknown.

We therefore propose a framework for calving models in which only H_0 and H_1 are specified, and strain rates, thickness gradient, and melt rates are allowed to evolve in time.

That is, a calving event is triggered when the terminus has thinned to the point that

$$H_t(x,y,t) = H_0(x,y,t), \tag{4.22}$$

and that once calving has begun the terminus retreats until

$$H_t(x,y,t) = H_1(x,y,t). \tag{4.23}$$

We suggest that this framework represents the simplest possible, universally-applicable calving framework.

$H_0(x,y,t)$ and $H_1(x,y,t)$ are difficult to define functions that potentially depend on a number of glaciological and oceanographic parameters, such as strain rates and crevasse spacing, ice temperature, pre-existing micro-fractures or "damage" [Pralong and Funk, 2005], melt water ponding on the glacier surface, terminus proximity to flotation, tides or other ocean swell, and resistance from a cover of pro-glacial sea ice or ice mélange. H_1 furthermore allows for self-sustaining calving processes, such as rapid stress transfer due to loss of resistance along the fjord walls or bottom, disintegration of the terminus by glaciogenic ocean waves [MacAyeal and others, 2009], or failure of a resistive ice mélange during the onset of a calving event [Amundson and others, 2010]. In other words, this framework allows calving events to be triggered at any point along the terminus; once triggered, self-sustaining processes can cause subsequent calving at distant points on the terminus or upglacier from the initial rupture.

In the following sections, H_0 and H_1 are left undefined but variations in H_0/H_1 are discussed in the context of different calving margins. We will argue that, for well-grounded glaciers, self-sustaining processes are unimportant and $H_0(t) \approx H_1(t)$. H_1 therefore primarily describes the structural rigidity of a floating terminus. If a terminus loses structural rigidity, possibly from the opening of large rifts due to thinning and flow acceleration [Joughin and others, 2008c] or to meltwater ponding on the glacier surface [Scambos and others, 2000], H_1 will become much larger than H_0 and the terminus will disintegrate.

Although H_0 and H_1 are not given here, they can be specified later with existing or newly-proposed calving theories. For example, the Van der Veen/Vieli and Benn calving

models amount to a specification of H_0 (in terms of terminus geometry in the former and crevasse depth in the latter) and the assumption that $H_1 \approx H_0$.

4.3.2 Case studies

Calving glaciers vary in flow speed, ice temperature, and geometry. Variations in these parameters give rise to differences in size and frequency of calving events. To investigate appropriate values for H_0/H_1, we group calving glaciers into five categories: fast-flowing and grounded (e.g., Alaska tidewater glaciers), fast-flowing and floating (e.g., many outlet glaciers in Greenland), lake calving, stable ice shelves, and unstable ice shelves. Typical near steady-state thickness gradients, calving event retreat lengths, strain rates, and periods between calving events for each of these groups, excluding unstable ice shelves, are indicated in Figures 4.2 and 4.3. Only approximate ranges are given, as statistics of calving margins are poorly known and documented (for some measured values see references in Benn and others [2007b], and also Sanderson [1979]; Joughin and others [2008a]; Alley and others [2008]; Amundson and others [2008]).

Calving events from grounded glaciers tend to be small but occur frequently [e.g., O'Neel and others, 2003, 2007], indicating that $H_0/H_1 \approx 1$. When near-terminus thinning rates (dynamic or melt-induced) are large relative to a glacier's calving rate, the terminus will go afloat and H_0/H_1 will decrease to 0.96–0.99, regardless of whether the terminus is cold and slow-flowing or temperate and fast-flowing (Figs. 4.2 and 4.3). Note that both temperate lake calving [Naruse and Skvarca, 2000; Warren and others, 2001; Boyce and others, 2007] and temperate tidewater glaciers (Columbia Glacier; personal communication from S. O'Neel, 2009) have been observed to develop short floating tongues. Values of $H_0/H_1 \approx 0.96$ may indicate that self-sustaining processes influence the size of calving events, whereas values closer to 0.99 may indicate that calving is controlled only by rift propagation. (Rift herein refers to a crevasse that penetrates the entire glacier thickness.)

In the calving framework, catastrophic disintegration of formerly intact, thin ice shelves over a period of days to weeks [Rott and others, 1996; Scambos and others, 2000; Braun

and others, 2009; Braun and Humbert, 2009] can occur either through changes in ice shelf thickness gradient or by decreasing H_0/H_1. Variations in ice shelf thickness gradient can be estimated by considering steady-state profiles of ice shelves. To generate steady-state profiles, we assume that $u = u_s$, that ice shelf density is constant, and that transverse variations in ice thickness and velocity are small. The steady-state mass continuity equation (Equation (4.9)) can be rearranged and oriented along a glacier flowline, such that

$$\frac{\partial h}{\partial x} = \frac{\dot{b} - h\dot{\varepsilon}_{xx}}{u}. \tag{4.24}$$

The longitudinal stretching rate is found by balancing the total force on any vertical column in the ice shelf with the horizontal force acting on the terminus [see Weertman, 1957; Sanderson, 1979], yielding

$$\dot{\varepsilon}_{xx} = A\left(\frac{1}{4}\rho_i g\left(1 - \frac{\rho_i}{\rho_w}\right)H - \frac{\tau}{2H}\int_x^L \frac{H}{w}dx\right)^n, \tag{4.25}$$

where A and n are flow law parameters and L is the total length of the ice shelf. Equations (4.24) and (4.25) can be solved by specifying a velocity and thickness at the grounding line, making an assumption about the value of the integral in Equation (4.25), integrating outward from the grounding line, and iterating until the ice shelf has the desired length [see explanation of methodology in Crabtree and Doake, 1982].

For an ice shelf with specified width, length, and flow law parameters, ice thickness is determined by thickness and velocity at the grounding line, surface and/or bottom melting, and shear stresses on the shelf margins. The geometry of the inner shelf is most strongly influenced by thickness and velocity at the grounding line, whereas the geometry of the outer shelf is determined by melt rates and shear stresses on the shelf margins (both assumed constant)(Fig. 4.4). Regardless of the input parameters, the near-terminus thickness gradient of a long ice shelf is nearly constant. Thus for a model to cause an ice shelf to collapse, H_0/H_1 must decrease considerably. Furthermore, processes that may condition an ice shelf for catastrophic failure, such as thinning due to increased melt rates or loss of shear stresses at the margin, may actually steepen the terminus and thereby reduce the likelihood that a high value of H_0/H_1 will cause the ice shelf to collapse. Steepening

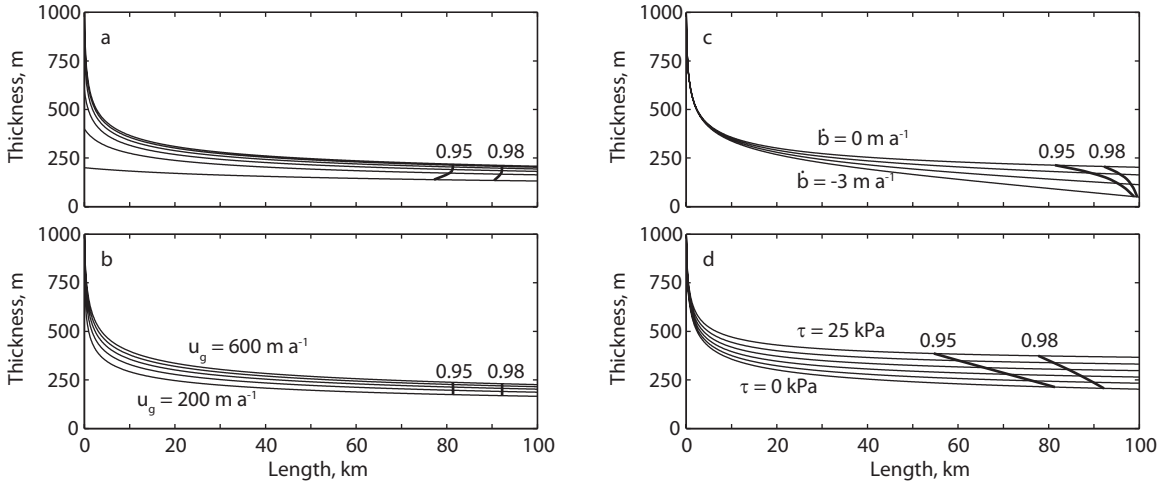

Figure 4.4. Theoretical steady-state thickness profiles of a 20 km wide and 100 km long ice shelf for various grounding line thicknesses and velocities (H_g and u_g), melt rates ($\dot{b}$), and lateral shear stresses (τ). (a) H_g =200–1200 m, u_g = 400 m a^{-1}, $\dot{b}$ = 0, and τ = 0. (b) H_g = 1000 m, u_g =200–600 m a^{-1}, $\dot{b}$ = 0, and τ = 0. (c) H_g = 1000 m, u_g = 400 m a^{-1}, $\dot{b}$ = -3–0 m a^{-1}, and τ = 0. (d) H_g = 1000 m, u_g = 400 m a^{-1}, $\dot{b}$ = 0, and τ = 0–25 kPa. In all plots the thick black curves indicate the points at which H_0/H_1 = 0.95 and H_0/H_1 = 0.98.

due to increased melting or loss of buttressing forces can initiate an irreversible retreat, however, as these processes would decrease terminus thickness and increase longitudinal strain rates (see Equation (4.17)).

4.3.3 Parameterization of self-sustaining processes

In light of the above observations, we propose a general relationship between H_0 and H_1 such that

$$H_1 = H_0(\mathbf{x_c}, ...) - \mathbf{x_c} \cdot \nabla h + \Gamma(\dot{b}, \dot{\varepsilon}_{xx}, \dot{\varepsilon}_{yy}, 1/H_0, T, H_g), \tag{4.26}$$

where $\mathbf{x_c}$ is crevasse spacing, $\Gamma \geq 0$ is a function that describes the effect of self-sustaining calving processes ($\Gamma = 0$ for grounded termini), T is ice temperature, and H_g is the ice thickness at the grounding line. For floating termini, calving flux may be primarily controlled by the propagation of widely-spaced rifts, and thus $\mathbf{x_c}$ refers to rift spacing.

The three terms on the right hand side of Equation (4.26) represent three poorly known

functions; identification of these functions would lead to a complete calving model. Previous work has focused primarily on identifying H_0 [Van der Veen, 1996; Vieli and others, 2000, 2001; Benn and others, 2007a,b]. Although the model of Benn and others [2007a,b] allows ice shelves to form, it does not take into account the potential role of crevasse spacing: if crevasses are widely spaced, then a terminus must reach flotation prior to calving. Although we do not propose an exact formulation of H_0, we do suggest that if $|\mathbf{x_c}|$ is large, then

$$H_0 \leq \frac{\rho_w}{\rho_i} H_w, \tag{4.27}$$

where H_w is the water depth at the terminus. Thus glaciers with large crevasse spacing (as proposed for lake calving glaciers [Venteris, 1999]) would be forced to go afloat prior to calving. This requirement does not necessarily force glaciers with small crevasse spacing to remain grounded. For example, if ice thickness is much greater than crevasse depth, crevasses may be ineffective at separating ice blocks from the glacier and a terminus can go afloat faster than it retreats back to the grounding line. In such cases calving rate may be more strongly controlled by the growth of deep rifts that penetrate the entire glacier thickness and produce large icebergs, such as those observed at Jakobshavn Isbræ. Furthermore, when crevasses are widely-spaced, calving events are triggered by the propagation of crevasses or rifts some distance $|\mathbf{x_c}|$ upglacier from the terminus. The thickness to which a terminus must thin prior to calving is therefore given by

$$H_0(\mathbf{x_c}, ...) = H_0(\mathbf{x_c} = 0, ...) + \mathbf{x_c} \cdot \nabla h. \tag{4.28}$$

Unfortunately the relationship between glacier stress field and crevasse and rift spacing is poorly known.

The second term in Equation (4.26) determines the size of a calving event when event size is determined exclusively by crevasse spacing (i.e., when self-sustaining processes are unimportant). This term is relatively large for slow-flowing glaciers such as lake calving glaciers and ice shelves, and close to zero for temperate tidewater glaciers.

Finally, the third term in Equation (4.26) describes the impact of self-sustaining processes and is only applicable to ice shelves. If an ice shelf has low strain rates and therefore

little damage, is thick, and/or cold, self-sustaining processes are unlikely to be important and therefore $\Gamma \approx 0$. Γ can increase if these properties change or if a strong melt season causes melt water to pond in crevasses and force the crevasses to grow downward [see Scambos and others, 2000]. Since self-sustaining processes cannot cause an ice shelf to retreat past its grounding line, $\Gamma \leq H_g - H_0$.

As a glacier advances or retreats over annual time scales, H_0/H_1 may vary quasi-periodically. For example, for a grounded tidewater glacier, $H_0/H_1 \approx 1$. As the terminus retreats and thins it may reach floatation, causing H_0/H_1 to decrease. If the newly-formed shelf is structurally rigid, H_0/H_1 may only decrease slightly (to $\sim$0.98) and the shelf will be a meta-stable feature that occasionally calves large icebergs. As the terminus continues to retreat and thin, the floating shelf may become unstable and $H_1 \rightarrow H_g$. The ice shelf will catastrophically collapse back to the grounding line, at which point $H_0/H_1 \rightarrow 1$.

Our calving framework does not preclude the formation of floating shelves during glacier advance. It does require, however, that for an ice shelf to develop during advance the terminus must be thick, slowly flowing (such that the ice is not highly damaged), and cold. Otherwise, self-sustaining processes (captured in Γ) will cause the shelf to collapse immediately after it forms. Possibly, expansive floating shelves are only a relict of retreating ice sheets. At the very least, the length that an ice shelf grows during advance is likely limited by the terminus thickness, which is a function of grounding line thickness and velocity [Sanderson, 1979].

4.4 Application of calving framework

The calving framework proposed in Section 4.3 is highly versatile and can easily incorporate new or existing calving models. To demonstrate we (1) use ad-hoc functions for H_0 and H_1 to produce seasonal variations in terminus behavior (Section 4.4.1) and (2) briefly discuss how the crevasse-depth calving criterion [Benn and others, 2007a,b] fits within the model framework (Section 4.4.2).

4.4.1 Seasonal variations in terminus position

Many tidewater glaciers experience large seasonal variations in terminus position and, in some cases, the size of and time interval between calving events [Meier and others, 1985; Motyka and others, 2003; Joughin and others, 2008b; Amundson and others, 2008, 2010]. Seasonal variations in terminus position can be attributed to variations in calving rate due to changes in thinning rate or thickness gradient, and to variations in backwards melting of the vertical face of the terminus, a process that also enables calving [Motyka and others, 2003; Röhl, 2006] (Equation (4.17)). Variations in the size of and interval between calving events, however, are better explained by processes controlling the ratio of pre- to post-calving terminus thickness (H_0/H_1; see Figs. 4.2 and 4.3).

To illustrate the effect of variations in H_0/H_1, we arbitrarily pick parameters to describe glacier flow (terminus velocity, strain rate, and thickness gradient are held constant) and let H_0 vary sinusoidally. Processes that might cause seasonal variations in H_0 include longitudinal stretching and surface melting, which affect crevasse depth near the terminus [e.g., Benn and others, 2007a,b], and variations in the strength of buttressing sea ice and/or ice mélange [Amundson and others, 2010]. In cases where calving ceases during winter, H_0 becomes effectively 0; in other words, no amount of thinning will cause the terminus to become unstable and calve.

We consider both the case in which H_1 is constant and so H_0/H_1 also varies with time, and the case in which $H_1(t) = H_0(t)$ (self-sustaining processes are unimportant). In the former, terminus position is determined by setting terminus velocity equal to some constant value and tracking the interval and size of calving events through Equations (4.12) and (4.15). In the latter, calving events occur continuously and are infinitesimally small; we thus use Equation (4.11) to calculate the instantaneous calving rate. The terminus position at a given time is then found by inserting Equation (4.11) into Equation (4.1) and integrating (Fig. 4.5).

When self-sustaining calving processes are important (i.e., $H_1(t) \neq H_0(t)$), seasonal variations in terminus position are amplified and the model produces fewer but larger calving

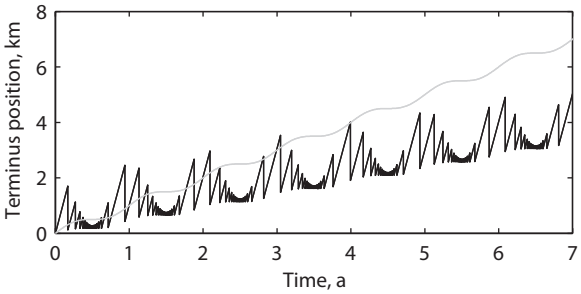

Figure 4.5. Terminus position versus time for a glacier with $u_t = 10$ km a^{-1}, $\dot{\varepsilon}_{zz} = -1$ a^{-1}, $\partial h/\partial x = -0.1$ (rough values for rapidly flowing outlet glaciers in Greenland), and $\dot{b} = \dot{m} = 0$. For both curves H_0 varies sinusoidally with an amplitude of 100 m and a mean value of $\overline{H_0} = 900$ m. The black and gray curves represent variations in terminus position for $H_1 = \max(H_0(t)) + 10$ m and $H_1(t) = H_0(t)$, respectively.

events in winter than in summer and slightly more calving events in spring than in fall. Furthermore, ignoring self-sustaining processes when they may be important can reduce the mean calving rate by several percent (as also indicated by Equations (4.17) and (4.18)). Our analysis has assumed, however, that terminus velocity is constant and unaffected by changes in terminus position, when in fact glacier velocity has been observed to change as a result of individual calving events [Amundson and others, 2008; Nettles and others, 2008]. Short-term changes in glacier flow associated with calving, which are poorly understood, can therefore influence long-term trends in terminus behavior. Furthermore, changes in the seasonal advance-retreat cycle can affect terminus stability and long-term behavior by enabling a terminus to advance to a stable pinning point in winter or to retreat past a pinning point in summer.

The seasonal variations in terminus position investigated here were driven by processes, such as changes in strength of a proglacial ice mélange [Joughin and others, 2008c; Amundson and others, 2010], that control the critical terminus thickness for calving, H_0. A glacier can, of course, experience variations in terminus position when H_0 is held constant. For example, submarine melting of a terminus affects terminus position by influencing the rate at which the terminus thins to H_0 and melts backward. The gray curve in Figure 4.5, produced by varying H_0 sinusoidally and assuming that $H_0 = H_1$, can also be produced

by holding H_0 constant and letting $\dot{b}$ vary from -100 m a^{-1} to +100 m a^{-1} (see Equation (4.11)). Ocean temperatures can therefore affect calving by (1) influencing the strength of proglacial ice mélanges through the growth and decay of interstitial sea ice, and (2) affecting the structural rigidity of the terminus (e.g., by controlling the crevasse depth to ice thickness ratio).

4.4.2 Incorporating existing calving criteria into the calving framework

Any thickness-based calving criterion can be incorporated into the calving framework with relative ease. For example, Benn and others [2007a,b] proposed that terminus position be located where the depth of a field of closely-spaced crevasses equals terminus freeboard, such that

$$H_0 = d_0 + W_0 + \delta_0, \tag{4.29}$$

d_0 is crevasse depth, W_0 is ice thickness minus glacier freeboard, and δ_0 represents the elevation (relative to sea level) of the bottom of the crevasse field at the onset of a calving event. In Benn and others [2007a,b], $\delta_0 = 0$; we prefer the more general formulation here, as it allows the critical crevasse depth to depend on other parameters such as ice temperature and damage.

For floating ice or grounded ice with widely-spaced crevasses, H_1 is given by Equation (4.26) or can be estimated by statistical analyses of calving margins and comparison to Figures 4.2 and 4.3. For grounded ice with closely-spaced crevasses, $H_1(t) \approx H_0(t)$ (see discussion in Section 4.3.2), and thus the steady-state calving rate (see Equation (4.11)) is given by

$$u_c = \frac{\left(\dot{b} + (d + \delta_0 + W_0)\dot{\varepsilon}_{zz}\right) \nabla h}{|\nabla h|^2} - \dot{m}. \tag{4.30}$$

The crevasse-depth calving criterion yields a steady-state calving rate that depends on water depth at the terminus, as first suggested by Brown and others [1982].

Other thickness-based calving models, such as the height-above-buoyancy calving criterion [Van der Veen, 1996; Vieli and others, 2000, 2001], can also be implemented in the calving framework with similar results. Identifying an appropriate function for H_0 and

determing the threshold at which $H_1 \rightarrow H_g$ (H_g is ice thickness at the grounding line), however, remain major tasks.

4.5 Conclusions

We have developed a framework for iceberg calving models based on (1) mass continuity, (2) the observation that, over annual time scales, terminus velocity and calving rate are generally much larger than changes in terminus position, suggesting a coupling between calving and flow parameters [Van der Veen, 1996], and (3) the simple idea that terminus thickness is larger following a calving event than immediately preceding the event. Our steady-state analysis indicates that calving rate is primarily governed by ice thickness, thickness gradient, dynamic thinning, and melting of the terminus; the analysis also provides a physical explanation for the empirical relationship for ice shelf calving found by Alley and others [2008]. Furthermore, variations in calving event size and periodicity can be prescribed simply by increasing the terminus thickness (by a few percent or less) during a calving event.

In the calving framework, terminus thicknesses at the onset of and immediately following calving events are given by two unknown but related functions. The functions may depend on strain rates and crevasse spacing, ice temperature, terminus proximity to flotation, tides or other ocean swell, and resistance from proglacial sea ice or ice mélange. Furthermore, differences between the functions determine how crevasse spacing and/or self-sustaining processes affect terminus behavior. For well-grounded glaciers with large crevasse spacing, the difference between the two functions depends only on crevasse spacing; if crevasse spacing is large, a terminus may need to achieve flotation prior to calving. On the other hand, the functions may differ significantly for floating termini that are thin, highly damaged, and/or warm; such termini are unstable to small perturbations and are therefore unlikely to be long-lasting features. With this calving framework, it may be difficult to develop expansive ice shelves during glacier advance, unless the glacier is thick, slowly flowing, and cold.

The calving framework we have developed does not constitute a complete calving model. It can, however, easily incorporate new or existing thickness-based calving models. The framework is sufficiently general to be applicable to all calving margins, yet sufficiently detailed to give insights into long-term terminus dynamics. Additionally, the form of the functions defining the framework can be investigated through, for example, statistical analyses of calving margins or numerical application of ad hoc functions. Most importantly, perhaps, the framework developed here provides a guide for future attempts to define a universal calving "law".

Finally, we note that glacier and ice sheet models are unable to characterize all calving processes in regions where calving events are small compared to the model grid spacing and/or changes in glacier flow occur on time scales much shorter than the model time step. Further work is need to assess and parameterize, if deemed necessary, the long term impact of rapid dynamical changes (such as those observed by Amundson and others [2008] and Nettles and others [2008]) associated with subgrid-scale calving events. .

Acknowledgments

This work was supported by NASA's Cryospheric Sciences Program (NNG06GB49G), the U.S. National Science Foundation (ARC0531075 and ARC0909552), and an International Polar Year student traineeship funded by the Cooperative Institute for Arctic Research (CIFAR) through cooperative agreement NA17RJ1224 with the National Oceanic and Atmospheric Administration. We thank E. Bueler, M. Fahnestock, M.P. Lüthi, R.J. Motyka, J. Brown, and D. Podrasky for discussions that inspired this work.

References

Alley, R.B., H.J. Horgan, I. Joughin, K.M. Cuffey, T.K. Dupont, B.R. Parizek, S. Anandakrishnan and J. Bassis. 2008. A simple law for ice-shelf calving. *Science*, **322**, 1344.

Amundson, J.M., M. Truffer, M.P. Lüthi, M. Fahnestock, M. West and R.J. Motyka. 2008. Glacier, fjord, and seismic response to recent large calving events, Jakobshavn Isbræ, Greenland. *Geophys. Res. Lett.*, **35**(L22501), doi:10.1029/2008GL035281

Amundson, J.M., M. Fahnestock, M. Truffer, J. Brown, M.P. Lüthi and R.J. Motyka. 2010. Ice mélange dynamics and implications for terminus stability, Jakobshavn Isbræ, Greenland. *J. Geophys. Res.*, **115**(F01005), doi:10.1029/2009JF001405.

Benn, D.I., N.R.J. Hutton and R.H. Mottram. 2007a. 'Calving laws', 'sliding laws' and the stability of tidewater glaciers. *Ann. Glaciol.*, **46**, 123–130.

Benn, D.I., C.R. Warren and R.H. Mottram. 2007b. Calving processes and the dynamics of calving glaciers. *Earth Sci. Rev.*, **82**, 143–179.

Boyce, E.S., R.J. Motyka and M. Truffer. 2007. Flotation and retreat of a lake-calving terminus, Mendenhall Glacier, southeast Alaska, U.S.A. *J. Glaciol.*, **53**(181), 211–224.

Braun, M., A. Humbert and A. Moll. 2009. Changes of Wilkins Ice Shelf over the past 15 years and inferences on its stability. *Cryosphere*, **3**, 41–56.

Braun, M. and A. Humbert. 2009. Recent retreat of Wilkins Ice Shelf reveals new insights in ice shelf breakup mechanisms. *Geosci. Rem. Sens. Lett.*, **6**(2), 263–267.

Brown, C.S., M.F. Meier and A. Post. 1982. Calving speed of Alaska tidewater glaciers, with application to Columbia Glacier, *USGS Prof. Pap.* 1258-C.

Crabtree, R.D. and C.S.M. Doake. 1982. Pine Island Glacier and its drainage basin: Results from radio echo-sounding. *Ann. Glaciol.*, **3**, 65–70.

De Angelis, H. and P. Skvarca. 2003, Glacier surge after ice shelf collapse. *Science*, **299**(1560), doi:10.1126/science.1077987.

Echelmeyer, K. and W.D. Harrison. 1990. Jakobshavns Isbræ, West Greenland: Seasonal variations in velocity — or lack thereof, *J. Glaciol.*, **36**(122), 82–88.

Hagen, J.O., K. Melvold, F. Pinglot and J.A. Dowdeswell. 2003. On the net mass balance of the glaciers and ice caps in Svalbard, Norwegian Arctic. *Arct. Antarct. Alp. Res.*, **35**(2), 264–270.

Howat, I.M., I. Joughin, M. Fahnestock, B.E. Smith and T.A. Scambos. 2008. Synchronous retreat and acceleration of southeast Greenland outlet glaciers 2000–06: ice dynamics and coupling to climate. *J. Glaciol.*, **54**(187), 646–660.

Jacobs, S.S., H.H. Helmer, C.S.M. Doake, A. Jenkins and R.M. Frolich. 1992. Melting of ice shelves and the mass balance of Antarctica. *J. Glaciol.*, **38**, 375–387.

Joughin, I., W. Abdalati and M. Fahnestock. 2004. Large fluctuations in speed on Greenland's Jakobshavn Isbræ glacier. *Nature*, **432**, 608–610.

Joughin, I., I. Howat, R. B. Alley, G. Ekstrom, M. Fahnestock, T. Moon, M. Nettles, M. Truffer and V. C. Tsai. 2008a. Ice-front variation and tidewater behavior on Helheim and Kangerdlugssuaq Glaciers, Greenland, *J. Geophys. Res.*, **113**(F01004), doi:10.1029/2007JF000837.

Joughin, I., S.B. Das, M.A. King, B.E. Smith, I.M. Howat and T. Moon. 2008b. Seasonal speedup along the western flank of the Greenland Ice Sheet. *Science*, **320**(5877), doi:10.1126/science.1153288.

Joughin, I., I.M. Howat, M. Fahnestock, B. Smith, W. Krabill, R.B. Alley, H. Stern and M. Truffer. 2008c. Continued evolution of Jakobshavn Isbræ following its rapid speedup, *J. Geophys. Res. - Earth Surface*, **113**(F04006), doi:10.1029/2008JF001023.

Lazzara M.A., K.C. Jezek, T.A. Scambos, D.R. MacAyeal and C.J. van der Veen. 1999. On the recent calving of icebergs from the Ross Ice Shelf. *Polar Geography*, **31**(1), 15–26.

MacAyeal, D.R., E.A. Okal, R.C. Aster and J.N. Bassis. 2009. Seismic observations of glaciogenic ocean waves (micro-tsunamis) on icebergs and ice shelves. *J. Glaciol.*, **55**(190), 193–206.

Meier, M.F., L.A. Rasmussen, R.M. Krimmel, R.W. Olsen and D. Frank. 1985. Photogrammetric determination of surface altitude, terminus position, and ice velocity of Columbia Glacier, Alaska. *U.S. Geol. Surv. Prof. Pap.*, 1258-F.

Motyka, R.J., L. Hunter, K.A. Echelmeyer and C. Connor. 2003. Submarine melting at the terminus of a temperate tidewater glacier, LeConte Glacier, Alaska, U.S.A. *Ann. Glaciol.*, **36**, 57–65.

Naruse, R. and P. Skvarca. 2000. Dynamic features of thinning and retreating Glaciar Upsala, a lacustrine calving glacier in southern Patagonia. *Arct. Antarct. Alp. Res.*, **32**(4), 485–491.

Nettles, M., T.B. Larsen, P. Elósegui, G.S. Hamilton, L.A. Stearns, A.P. Ahlstrøm, J.L. Davis, M.L. Andersen, J. de Juan, S.A. Khan, L. Stenseng, G. Ekström and R. Forsberg. 2008. Step-wise changes in glacier flow speed coincide with calving and glacial earthquakes at Helheim Glacier, Greenland. *Geophys. Res. Lett.*, **35**(L24503), doi:10.1029/2008GL036127.

O'Neel, S., K.A. Echelmeyer and R.J. Motyka. 2003. Short-term variations in calving of a tidewater glacier: LeConte Glacier, Alaska, U.S.A. *J. Glaciol.*, **49**(167), 587–598.

O'Neel, S., H.P. Marshall, D.E. McNamara and W.T. Pfeffer. 2007. Seismic detection and analysis of icequakes at Columbia Glacier, Alaska. *J. Geophys. Res.*, **112**(F03S23), doi:10.1029/2006JF000595.

Pfeffer, W.T. 2007. A simple mechanism for irreversible tidewater glacier retreat. *J. Geophys. Res.*, **112**, F03S25, doi:10.1029/2006JF000590.

Pralong, A. and M. Funk. 2005. Dynamic damage model of crevasse opening and application to glacier calving. *J. Geophys. Res.*, **110**(B01309), doi:10.1029/2004JB003104.

Rignot, E., G. Casassa, P. Gogineni, W. Krabill, A. Rivera and R. Thomas. 2004. Accelerated ice discharge from the Antarctic Peninsula following the collapse of Larsen B ice shelf. *Geophys. Res. Lett.*, **31**(L18401), doi:10.1029/2004GL020697.

Rignot, E. and P. Kanagaratnam. 2006. Changes in the velocity structure of the Greenland Ice Sheet. *Science*, **311**(5763), 986–990, doi:10.1126/science.1121381.

Röhl, K. 2006. Thermo-erosional notch development at fresh-water-calving Tasman Glacier, New Zealand. *J. Glaciol.*, **52**(177), 203–213.

Rott, H., P. Skvarca and T. Nagler. 1996. Rapid collapse of northern Larsen Ice Shelf, Antarctica. *Science*, **271**(5250), 788–792.

Sanderson, T.J.O. 1979. Equilibrium profile of ice shelves. *J. Glaciol.*, **22**(88), 435–460.

Scambos, T., C. Hulbe, M. Fahnestock and J. Bohlander. 2000. The link between climate warming and break-up of ice shelves in the Antarctic Peninsula. *J. Glaciol.*, **46**(154), 516–530.

Van der Veen, C.J. 1996. Tidewater calving. *J. Glaciol.*, **42**(141), 375–385.

Venteris, E.R. 1999. Rapid tidewater glacier retreat: a comparison between Columbia Glacier, Alaska and Patagonian calving glaciers. *Global Planet. Change*, **22**, 131–138.

Vieli, A., M. Funk and H. Blatter. 2000. Tidewater glaciers: frontal flow acceleration and basal sliding. *Ann. Glaciol.*, **31**, 217–221.

Vieli, A., M. Funk and H. Blatter. 2001. Flow dynamics of tidewater glaciers: a numerical modelling approach. *J. Glaciol.*, **47**(59), 595–606.

Warren, C., D. Benn, V. Winchester and S. Harrison. 2001. Buoyancy-driven lacustrine calving, Glaciar Nef, Chilean Patagonia. *J. Glaciol.*, **47**(156), 135–146.

Weertman, J. 1957. Deformation of floating ice shelves. *J. Glaciol.*, **3**(21), 38–42.

Chapter 5

Conclusions

Calving at Jakobshavn Isbræ is highly seasonal, causing the terminus to advance and retreat several kilometers each year. In winter the dense mélange of icebergs and sea ice in the fjord strengthens and prevents icebergs from calving, even if crevasses have propagated through the entire glacier thickness. In summer the mélange weakens and the terminus retreats.

Mass losses from calving are dominated by the subweekly calving of full-glacier-thickness icebergs. Such calving events typically involve the successive detachment and overturning of several icebergs; the first icebergs to calve (during a calving event) always rotate bottom out from the terminus, whereas subsequent icebergs can rotate any direction or remain tabular (upright). Tabular icebergs are only calved in early summer, suggesting that by mid-summer the terminus has retreated to a near grounded position, which is further corroborated by a lack of vertical tidal motion of survey markers deployed on the lower glacier. On the other hand, simple theoretical considerations demonstrate that full-glacier-thickness icebergs cannot calve from a well-grounded terminus, thus indicating that the glacier's retreat rate is limited by its proximity to flotation.

These calving events have a substantial impact on their surroundings: they produce ocean waves and seismic signals (including "glacial earthquakes") that can be detected more than 50 km and 250 km from the terminus, respectively, cause icebergs in the fjord to move 2 km in an hour, and cause the lower glacier to accelerate by $\sim$3% by redistributing stresses within the glacier. The events do not cause episodic glacier slip, however, thus contradicting the initially proposed glacial earthquake mechanism.

Motion of the proglacial ice mélange is strongly modulated by calving events. Between events, including the entire winter, the mélange is pushed down fjord as a cohesive unit by the advancing terminus. Motion of the mélange becomes highly episodic during periods of high calving activity, when large calving events cause the mélange to rapidly move 2–4 km down fjord, extend longitudinally, and be subjected to vertical oscillations lasting

over 12 hrs and having peak amplitudes greater than 1 m. The vertical oscillations may promote further disintegration of the terminus and ice mélange, resulting in additional seaward expansion and thinning of the mélange. After a calving event the mélange rapidly decelerates over a period of roughly 30 minutes.

Our observations and simple force balance analysis demonstrate that the mélange also influences calving behavior: the first icebergs to calve tend to be small and always rotates bottom out, whereas subsequent calving icebergs can be larger and rotate any direction. Motion of the mélange away from the terminus does not appear to be prerequisite for calving to begin. However, when the mélange is activated during calving onset, it loses the ability to resist the calving of subsequent icebergs. The total amount of ice lost during a calving event is therefore likely controlled by parameters other than mélange strength, such as the presence (or absence) of pre-existing rifts up-glacier. Thus it is unlikely that the ice mélange controls the net calving flux in summer over time periods of days to weeks. Over seasonal time scales or longer, the mélange could influence the net calving flux by controlling the proportion of the year during which calving can occur. Although the resistive force from the mélange may be insufficient to directly influence glacier motion, the mélange may indirectly influence glacier dynamics by controlling the evolution of the terminus geometry, which in turn affects glacier motion.

The style of calving observed at Jakobshavn Isbræ, and presumably similar glaciers in Greenland, appears to represent a previously undescribed class of calving glaciers. For comparison, mass loss from calving at expansive ice shelves in Antarctica is dominated by the decadal calving of kilometer-scale icebergs, while mass loss from calving at grounded temperate glaciers is typically dominated by the (roughly) hourly calving of meters-scale icebergs. Our observations led to the development of a simple framework for calving models that can be applied to any calving margin. The framework is based on mass continuity, the observation that calving rate tends to scale with terminus velocity, and the simple idea that terminus thickness increases during a calving event. Several different styles of calving can be prescribed simply by setting the ratio of the pre- and post-calving terminus thick-

nesses to 0.96–0.99, regardless of glacier temperature, proximity to flotation, flow field, and geometry. Larger variations in calving behavior can be prescribed by allowing for the ratio of pre- to post-calving terminus thickness to vary in space and time. Although the framework does not provide a complete calving model, it does provide a guide for future studies of calving. Furthermore, analysis of the framework suggests that calving rate is controlled, to first order, by strain rate, thickness gradient, terminus thickness, and melting of the terminus.

Outlook

The biggest gains in understanding of calving processes have come by watching calving events unfold. As technology has improved, so have our observations. By combining satellite imagery, high-rate digital photography and video, and seismic data, it is now possible to build a highly detailed inventory of calving events from any number of calving margins. Such an inventory, when put into the context of a simple calving framework such as the one proposed here, will undoubtedly lead to an improvement in calving models.

On the other hand, certain processes that influence calving are difficult to ascertain from observations alone. In particular, information on crevasse propagation rates and crevasse spacing would be highly useful, but may be most readily addressed with numerical modeling exercises. Similarly, fjord conditions and their impact on terminus dynamics are often difficult to assess from field measurements alone.

An additional complication arising from this and other previous work is that calving is driven by processes occurring close to a glacier terminus. Large-scale ice sheet models, however, typically have grid spacings and time steps that are too large to adequately describe individual calving events and associated changes in glacier flow and geometry. The long-term impact of these dynamic changes is presently unknown but may be significant. Future attempts to parameterize calving should also take into account time-dependent variations in near-terminus flow associated with calving.

References

Abdalati, W., W. Krabill, E. Frederick, S. Manizade, C. Martin, J. Sonntag, R. Swift, R. Thomas, W. Wright, and J. Yungel (2001), Outlet glacier and margin elevation changes: Near-coastal thinning of the Greenland Ice Sheet, *J. Geophys. Res.*, *106*(D24), 33729–33741.

Alley, R.B., H.J. Horgan, I. Joughin, K.M. Cuffey, T.K. Dupont, B.R. Parizek, S. Anandakrishnan, and J. Bassis (2008), A simple law for ice-shelf calving, *Science*, *322*, 1344.

Benn, D.I., N.R.J. Hutton, and R.H. Mottram (2007a), 'Calving laws', 'sliding laws' and the stability of tidewater glaciers, *Ann. Glaciol.*, *46*, 123–130.

Benn, D.I., C.R. Warren, and R.H. Mottram (2007b), Calving processes and the dynamics of calving glaciers, *Earth Sci. Rev.*, *82*, 143–179.

Bindschadler, R.A. (1984), Jakobshavns Glacier drainage basin: A balance assessment, *J. Geophys. Res.*, *89*(C2), 2066–2072.

Birnie, R.V. and J.M. Williams (1985), Monitoring iceberg production using LANDSAT, *Proceedings of the University of Dundee Summer School*, European Space Agency SP-216, 165–167.

Braun, M., A. Humbert, and A. Moll (2009), Changes of Wilkins Ice Shelf over the past 15 years and inferences on its stability, *Cryosphere*, *3*, 41–56.

Braun, M. and A. Humbert (2009), Recent retreat of Wilkins Ice Shelf reveals new insights in ice shelf breakup mechanisms, *Geosci. Rem. Sens. Lett.*, *6*(2), 263–267.

Brown, C.S., M.F. Meier, and A. Post (1982), Calving speed of Alaska tidewater glaciers, with application to Columbia Glacier, *USGS Prof. Pap.* 1258-C.

Cathles, L. M., IV, E.A. Okal, and D.R. MacAyeal (2009), Seismic observations of sea swell on the floating Ross Ice Shelf, Antarctica, *J. Geophys. Res.*, *114*, F02015, doi:10.1029/2007JF000934.

Csatho, B., T. Schenk, C.J. Van der Veen, and W.B. Krabill (2008), Intermittent thinning of Jakobshavn Isbræ, West Greenland, since the Little Ice Age, *J. Glaciol.*, *54*(184), 131–144.

De Angelis, H. and P. Skvarca (2003), Glacier surge after ice shelf collapse, *Science*, *299*(1560), doi:10.1126/science.1077987.

Geirsdóttir, Á., G.H. Miller, N.J. Wattrus, H. Björnsson, and K. Thors (2008), Stabilization of glaciers terminating in closed water bodies: Evidence and broader implications, *Geophys. Res. Lett.*, *35*(L17502), doi:10.1029/2008GL034432.

Higgins, A.K. (1991), North Greenland glacier velocities and calf ice production, *Polarforschung*, *60*(1), 1–23.

Holland, D.M., R.H. Thomas, B. DeYoung, M.H. Ribergaard, and B. Lyberth (2008), Acceleration of Jakobshavn Isbræ triggered by warm subsurface ocean waters, *Nature Geoscience*, *1*, 659–664, doi:10.1038/ngeo316.

Howat, I.M., I. Joughin, M. Fahnestock, B.E. Smith, and T.A. Scambos (2008), Synchronous retreat and acceleration of southeast Greenland outlet glaciers 2000–06: ice dynamics and coupling to climate, *J. Glaciol.*, *54*(187), 646–660.

Joughin, I., W. Abdalati, and M. Fahnestock (2004), Large fluctuations in speed on Greenland's Jakobshavn Isbræ glacier, *Nature*, *432*, 608–610, doi:10.1038/nature03130.

Lazzara M.A., K.C. Jezek, T.A. Scambos, D.R. MacAyeal, and C.J. van der Veen (1999), On the recent calving of icebergs from the Ross Ice Shelf, *Polar Geography*, *31*(1), 15–26.

Motyka, R.J., L. Hunter, K.A. Echelmeyer, and C. Connor (2003), Submarine melting at the terminus of a temperate tidewater glacier, LeConte Glacier, Alaska, U.S.A., *Ann. Glaciol.*, *36*, 57–65.

O'Neel, S., K.A. Echelmeyer, and R.J. Motyka (2003), Short-term variations in calving of a tidewater glacier: LeConte Glacier, Alaska, U.S.A., *J. Glaciol.*, *49*(167), 587–598.

O'Neel, S., H.P. Marshall, D.E. McNamara, and W.T. Pfeffer (2007), Seismic detection and analysis of icequakes at Columbia Glacier, Alaska, *J. Geophys. Res.*, *112*(F03S23), doi:10.1029/2006JF000595.

Podlech, S. and A. Weidick (2004), A catastrophic break-up of the front of Jakobshavn Isbræ, West Greenland, 2002/2003, *J. Glaciol.*, *50*(168), 153–154.

Reeh, N., H.H. Thomsen, A.K. Higgins, and A. Weidick (2001), Sea ice and the stability of north and northeast Greenland floating glaciers, *A. Glaciol.*, *33*, 474–480.

Rignot, E., G. Casassa, P. Gogineni, W. Krabill, A. Rivera, and R. Thomas (2004), Accelerated ice discharge from the Antarctic Peninsula following the collapse of Larsen B ice shelf, *Geophys. Res. Lett.*, *31*(L18401), doi:10.1029/2004GL020697.

Rott, H., P. Skvarca, and T. Nagler (1996), Rapid collapse of northern Larsen Ice Shelf, Antarctica, *Science*, *271*(5250), 788–792.

Scambos, T., C. Hulbe, M. Fahnestock, and J. Bohlander (2000), The link between climate warming and break-up of ice shelves in the Antarctic Peninsula, *J. Glaciol.*, *46*(154), 516–530.

Thomas, R.H. (1979), Ice shelves: A review, *J. Glaciol.*, *24*(90), 273–286.

Thomas, R.H., W. Abdalati, E. Frederick, W.B. Krabill, S. Manizade, and K. Steffen (2003), Investigation of surface melting and dynamic thinning on Jakobshavn Isbræ, Greenland, *J. Glaciol.*, *49*(165), 231–239.

Truffer, M. and M. Fahnestock (2007), Rethinking ice sheet time scales, *Science*, *315*(5818), doi: 10.1126/science.1140469.

Van der Veen, C.J. (1996), Tidewater calving, *J. Glaciol.*, *42*(141), 375–385.

Vieli, A., M. Funk, and H. Blatter (2000), Tidewater glaciers: frontal flow acceleration and basal sliding, *Ann. Glaciol.*, *31*, 217–221.

Vieli, A., M. Funk, and H. Blatter (2001), Flow dynamics of tidewater glaciers: a numerical modelling approach, *J. Glaciol.*, *47*(59), 595–606.